

## **Converted-wave seismic exploration: a tutorial**

Robert R. Stewart, James E. Gaiser, R. James Brown, and Don C. Lawton

### **ABSTRACT**

Multicomponent seismic recording (measurement with vertical and horizontal geophones and possibly a hydrophone or microphone) captures the seismic wavefield more completely than with conventional single element techniques. In the last several years, multicomponent surveying has developed rapidly – allowing creation of converted-wave or P-S images that make use of a downgoing P wave converting to an upgoing S wave at the deepest point of penetration. Survey design for P-S surveys is similar to that of P waves, but must take into account the P-S wave's asymmetric raypath. P-S surveys use conventional sources but have several times more recording channels. Some special processes for P-S analysis include anisotropic rotations, shear receiver statics, asymmetric and anisotropic binning, shifted hyperbolic velocity analysis, P-S to P-P time transformation, P-S DMO, pre- and post-stack migration, and stacking velocity and reflectivity inversion for S velocities.

Current P-S sections are approaching (and in some cases exceeding) the quality of conventional P-P seismic data. Interpretation of P-S sections uses elastic ray tracing, synthetic seismograms, correlation with P-wave sections and depth migration. Numerous applications for P-S sections have arisen including sand/shale differentiation, carbonate identification, definition of interfaces with low P-wave contrast, anisotropic analysis, imaging through gas zones, and reservoir monitoring. Marine converted-wave analysis using 4-C recordings (a three-component geophone plus a hydrophone) has generated some remarkable images. Imaging through high-velocity layers (e.g. salt, basalt, permafrost) and in regions of significant structure also look promising. Development of the P-S method has taken about 15 years, but has now entered into its commercial phase.

### **BACKGROUND**

The primary method of hydrocarbon exploration remains P-wave seismic reflection surveying – and for good reason. Among all the elastic waves, compressional waves arrive first, usually have high signal-to-noise values, have particle motion that is close to rectilinear, are easily generated by a variety of sources, and propagate in a marine environment. We expect that P-wave reflection surveying will be the dominant exploration method for some years to come. But, several questions are germane: Can we improve P-wave pictures? Can we generate complementary or augmenting images? When P-wave surveying fails, can we use other seismic techniques? Perhaps the most straightforward answer to these questions is yes, try multicomponent recording and analysis. There is considerable promise in using multicomponent recordings to improve P-wave data. However, the thrust of this paper is to provide an introduction to converted-wave seismic exploration.

By converted-wave exploration, we are specifying a particular conversion – a P wave propagating downward, converting to an S wave at the deepest point of penetration and coming back upward (see Figure 1). We note here that the asymmetry of the raypath is described in Snell's Law:  $(\sin \theta)/V_p = (\sin \phi)/V_s$ ; and as  $V_s < V_p$ ,  $\phi$  is then less than  $\theta$ . Thus, the wave travels more vertically coming up than going down.

While Snell's Law gives the basic geometry of the raypaths, the Zoeppritz equations provide the amplitudes of the reflections. For the simple case in Figure 2, we note the sinusoidal growth in the converted-wave reflectivity. Aki and Richards (1980) show that P-S reflectivity can be written approximately (assuming property changes are small) as:

$$R = -k \left[ (1 + \delta) \frac{\Delta \rho}{\rho} + 2\delta \frac{\Delta V_s}{V_s} \right],$$

where

$$k = (\gamma \tan \phi)/2,$$

$$\delta = -2(\sin^2 \theta)/\gamma^2 + 2(\cos \theta \cos \phi)/\gamma,$$

$$\gamma = V_p/V_s.$$

There are several notable aspects of this equation: (i) it has no dependence on P-wave velocity change; (ii) it is negative for positive parameter changes up to moderate angles; (iii) it indicates similar amounts of P-S energy, at moderate angles, when compared to the P-P energy given by the corresponding P-P reflectivity (Figure 2).

There are many other types of energy conversion that may occur as seismic waves propagate in the Earth. In relatively high-velocity layers, such as permafrost, volcanics or salt, there may be an S-wave leg generated in the downgoing path that converts back to a P wave. In the marine case, we might have a P-to-S downgoing conversion at the ocean bottom that will reflect as an S wave (Tatham, 1982). Nonetheless, multiple conversions will generally have much lower amplitudes than the primary P-to-S reflection.

Concentrated work in P-S analysis has been proceeding for about 15 years. There are now a number of commercial acquisition and processing groups. We might compare this with the development of 3-D seismology using P waves. The 3-D seismic concept and early experimentation came about in the 1960s, theory and processing largely worked out in the 70s, and application in the 80s – about 20 years from concept to common practice. P-S surveying was proposed and tried in the early 1980s with processing fundamentals developed in the late 1980s to early 1990s. Assuming P-S surveying is on a similar track as was 3-D seismic analysis, we would expect it to be common in the next several years.

We might inquire why multicomponent and especially P-S methodologies haven't been widely used in the past. There are likely a number of reasons for this. In the

acquisition world of several years ago, 3-C geophones were not available in large numbers. There were challenging logistics in planting and cabling them, and in their recording – with three times the normal number of channels. Converted-wave survey design was not well understood and design software not commercially available.

Processing P-S waves was also problematic as much of the theory for processing the data had not been developed. The curved trajectory of the P-S wave reflection point (Figure 3), due to unequal incidence and reflection angles, was a major stumbling block for conventional analysis. Again, software was not available.

Furthermore, interpreting P-S data was difficult because few S-wave velocity logs had been acquired and P-S synthetic seismograms were not available. On top of all this, P-P and P-S sections displayed events, from the same reflector, at different times! Finally, there were few definitive case histories. In other words, the method was in its early infancy.

Now, however, almost all of this has changed. There are P-S survey-design programs, geophones and recording channels are generally available, and logistics are better practised. Several commercial processing packages and contractors handle P-S processing. In addition, S-wave logging is more commonly conducted and interpretative software is available. And we're building some impressively successful case histories.

So, if the broad goal of seismic exploration is to create a 3-D depth image of rock type, structure, and saturant, then we will need all the information that is available through the seismic method. Again, we are unlikely to be able to do this with P waves alone. This is because different rocks and saturants can have a similar P-wave response. Furthermore, some interfaces may have low P-wave contrast. However, S-wave properties may well vary, and along with the P-wave properties, can help characterize the rock structure, type, and fluids therein. In more detail then, how can we obtain S-wave properties from surface seismic measurements?

We can attempt to find S-wave information via amplitude-versus-offset (AVO) analysis of P-P data. AVO is useful in some areas, but often limited due to its second-order dependence of P-wave reflectivity on S-wave velocity. In addition, there are signal-to-noise and processing problems with AVO analysis (Arnold and Chiburis, 1998) and issues of calibration, anisotropy, attenuation, thin-bed tuning, and multipathing. We also use limited and perhaps oversimplified models to relate AVO response to rock properties. Furthermore, our most fundamental seismic measurement is that of event times. AVO analysis does not give us S-wave traveltimes. P-S surveys do. The P-S time structure and isochron maps can be used with the P-P section to extract  $V_P/V_S$  values.

Pure-shear surface-seismic surveys are also possible and have been used. They directly measure S-wave parameters. Unfortunately, S-S seismic sections are often noisy and can have low resolution – partially because of the two-way propagation path of the S waves through the usually attenuative, low-velocity, and heterogeneous near-surface. Furthermore S-wave sources are expensive, scarce, and not easily

applicable in some environments (e.g., marine settings, transition zones, muskeg, and environmentally sensitive areas). In addition, S-S listening times in recording are double those of P waves and about 30% longer than for converted waves. All totalled, pure S-wave surveys usually cost more than acquiring P-S data (Kendall and Davis, 1996). Thus, expense and data quality have limited the applicability of S-S surveys.

P-S surveys are a relatively inexpensive, broadly applicable, and effective way to obtain S-wave information. If we do have P-S reflectivity, what can it be used for?

- Providing another section with independent properties (e.g., velocity, multiples, tuning).
- More detailed shallow imaging.
- Imaging interfaces with low P-wave contrast but significant S-wave change.
- Imaging through gas chimneys, shale diapirs, and mud volcanoes.
- Assisting P-P interpretation via  $V_p/V_s$  analysis and correlation.
- Augmenting conventional AVO analysis.
- Investigating anisotropy as well as fracture density and orientation.
- Calibrating P-wave bright spots.
- Using  $V_p/V_s$  for lithology (e.g., sand/shale).
- Imaging high-angle faults.
- Monitoring reservoir changes.

Let's look at some of the tools that have been developed for S-wave work.

## TOOLS OF THE TRADE

### Elastic-wave logs

Full-waveform sonic logs give information about both P-wave and S-wave velocities (Mari et al., 1994). Transmitted tube waves from a monopole source, flexural waves from dipole sources, and screw modes from quadrupole sources can all be used to estimate the formation shear velocity under various conditions. Cross-dipole logs (where the source and receivers are not parallel) have been used to estimate anisotropy (Xu and Parra, 1998).

The basis of much of the lithologic work in P-S exploration relates to anomalous changes in  $V_s$  with respect to  $V_p$ . A changing  $V_p/V_s$  value is often closely tied to a changing lithology. For example, Miller and Stewart (1990) use data from full waveform sonic logs in the Medicine River field in Alberta to analyse  $V_p/V_s$  ratios from pure lithologies (sandstone, shale, limestone – Figure 4a). Similar to values reported by other authors, their  $V_p/V_s$  values for sandstone cluster around 1.6, with higher values near 1.9 for shales and limestone. When the lithologies become mixed or complex, the  $V_p/V_s$  values change to more intermediate quantities (Figure 4b).

Miller (1996) also shows log values from a field in southern Alberta (Figure 5). The Glauconitic sandstone reservoir shows significantly higher  $V_S$  values than from the off-reservoir shales at the same depth. Thus, we expect a decrease in  $V_P/V_S$  from regional shales to reservoir sand. We can also plot these data as  $V_P/V_S$  versus gamma-ray values. Generally, there is a small increase in  $V_P/V_S$  for sands with more clay or shaliness. Shales themselves have significantly higher  $V_P/V_S$  values than these sands.

Similarly, in analysing an array sonic log from the Davey well (3-13-34-29W4) in central Alberta, Miller (1992) plotted  $V_P/V_S$  values, PEF (photoelectric cross-section) curves, and anhydrite fraction (Figure 6). The other primary lithology was dolomite. She noted that  $V_P/V_S$  from the array sonic tracks the PEF curve and volume of anhydrite quite well – as the anhydrite versus dolomite fraction increases so do the  $V_P/V_S$  and PEF logs. Anhydrite values are about 2.0; dolomites are about 1.85. Figure 7, shows the correlation of  $V_P/V_S$  with dolomite (1.85) and limestone (1.95). Again, as the limestone fraction versus dolomite increases so do the  $V_P/V_S$  and PEF logs.

The log values also form the basis for generating synthetic seismograms, which assist in interpreting P-P and P-S sections. Lawton and Howell (1992) developed a procedure to calculate one-dimensional P-S synthetic seismograms. Examples of P- and S-velocity logs and their corresponding P-P and P-S synthetic seismograms from the Blackfoot area of Southern Alberta are shown in Figure 8.

We recall that elastic-wave velocities and impedances can be related to various combinations of density and the Lamé parameters. For example, P-wave and S-wave impedances,  $I_p$  and  $I_s$ , can be written as  $I_p^2 = (\rho V_p)^2 = (\lambda + 2\mu)\rho$  and  $I_s^2 = (\rho V_s)^2 = \mu\rho$ , where  $\mu$ ,  $\lambda$  are the Lamé parameters and  $\rho$  is the density. Goodway et al. (1997) write  $\lambda\rho = I_p^2 - 2I_s^2$  and suggest that analysis of  $\lambda\rho$  and  $\mu\rho$  can provide excellent indicators of pore fluids.

### VSP surveys

VSP surveys generally use 3-C geophones and have done so for many years. This is partially a result of using offset sources that generate clear P and S energy on both horizontal and vertical channels (Figure 9). Competent deep rock usually has high velocity that allows waves to propagate at large angles from the vertical direction. This is different from the surface seismic case where the generally low-velocity near-surface bends raypaths to the vertical. On the surface, this places P waves largely on the vertical geophone and S waves on the horizontal elements. In the VSP case, multicomponent analysis with 3-C recording is usually required to disentangle the P- and S-wave energy on both channels. Interestingly, VSP processing had an impact on P-S surface analysis: P-wave reflection points from a given source to a specific VSP receiver form a curved line in depth – they do not fall on a straight common mid-point line (Figure 10a). Note that the P-S reflection trajectories in the VSP geometry are also curved and pushed toward the receivers (Figure 10b). Such is also the case with the P-to-S conversion for a surface source and receiver (Figure 3). The VSP case helped researchers understand of how to do common-conversion-point (CCP) mapping for P-S data in a surface geometry.

A basic aim of the VSP survey is to determine seismic interval velocities. From the traveltime of the first-breaking energy in depth, we can calculate velocities. An example from the Hamburg area of central Alberta is shown in Figure 11. We note the low  $V_p/V_s$  value of the porous dolomite with respect to the surrounding limestones. In addition, the seismic velocities are generally lower than sonic values as we would expect from attenuation-dispersion arguments.

We can also assemble well logs, VSP data, synthetic seismograms, and surface seismic into a compelling display called a composite plot or L plot. This is a very useful compendium of correlated data that often allows a more confident interpretation. An example is the composite plot from the Rolling Hills of southern Alberta shown in Figure 12 (Geis et al., 1990). Note the good correlation of events across the various data types. Throughout the recording and processing sequence, it is critical to keep polarities consistent. This is accomplished by using SEG recommended field polarities and the Aki and Richards (1980) energy-partitioning equations. Generally, when we do this, both P-P and P-S final zero-phase sections will have trace peaks corresponding to P- and S-impedance increases. In the subsurface, P-P and P-S events have about the same frequency content (Figure 13). Unfortunately however, by the time the P-S events are recorded at the surface, their frequency has often decreased relative to that of the P wave (Figure 14).

Another example of P-P and P-S VSP data comes from the Willesden Green region of central Alberta (Figure 15). We see much more reflection activity in the shallow part of the P-S section as compared to the P-P section (Stewart et al., 1995). In this case, both sections have been plotted in P-wave time (effectively, both sections are processed to depth then converted back to P-wave time).

Coulombe et al. (1996) used VSP measurements to analyse AVO effects in a carbonate section. They found that P-S and P-P AVO effects were in evidence and could be modelled (Figures 16 and 17). In the VSP data, the P-S section gave a higher resolution picture in which the top and bottom of the porous zone could be identified.

In another case of P-S imaging at Judy Creek, Alberta (Campbell et al., 1994), both P-P and P-S images helped identify a porosity development that the well had missed (Figure 18).

### **Multicomponent surface-seismic acquisition**

One of the earliest discussions concerning the surveying, analysis, and interpretation of converted waves was published by Garotta et al. (1985). They used a two-element (vertical and horizontal) geophone for acquisition. The data recorded were quite good. Nevertheless, we would now generally recommend using a three-component geophone so that off-line effects, misorientation, anisotropy, crooked lines, and 3-D shooting can be handled.

Lawton and Bertram (1993) tested four 3-C geophones, using a source at various azimuths to the receivers. The goal of this survey was to determine if the output response (hodograms) of the horizontal elements would indicate the direction of the

source from the receiver; that is, if the geophone response would faithfully reproduce anticipated particle motion. They found that the three geophones currently on the market all performed well. This was important for further establishing the fidelity of the field measurements before proceeding on to sophisticated processing. Eaton and Lawton (1992) analysed the fold of a 2-D P-S section and found it to be oscillatory under certain conditions. To avoid this problem, they recommend using a source or shot-line interval with an odd-integer multiple of the receiver spacing multiplied by the  $V_p/V_s$  value. That is,  $SI/RI = nV_p/V_s$ , where  $n$  is odd. Additional processes such as adjacent-trace averaging, depth- and velocity-variant binning, and DMO can also help in smoothing the final fold.

Lawton et al. (1995) discuss the design of 3C-3D surveys. They again show the need to carefully consider converted-wave design to avoid having lines or regions of low fold.

### **Acquisition limitations**

The recording of land and marine multicomponent 3-C data is still somewhat constrained by several factors. Three-component geophones and 4-C cables have sometimes been in short supply. As demand continues to increase, more geophones are being built. Because of the current need on land to orient the geophones carefully, field layout and planting can be a time-consuming process. It would be useful to have a geophone that could automatically level or orient itself. Gimballed devices are used in VSP surveys as well as in marine cables. Auto-orienting surface geophones are under development.

There are still issues about the use of arrays or single phones that need to be resolved with careful fieldwork and processing. However, several tests on land indicate that by the final migrated section stage, there is little difference between single-phone and array data. In fact, arrays may actually damage the P-S data due to large and rapidly varying statics (Hoffe et al., 1999). Generally, buried geophones are thought to provide a better signal with less noise. We generally have used 3-C geophones in augured holes about 0.3 m deep. To test the effect of a deeper plant, we shot two test lines with buried 3-C geophones up to 18-m depth. Somewhat surprisingly to us, we have not found an improvement in data quality. This may be due, in part, to the difficulty in obtaining a good 3-C plant in a drilled hole.

Other issues for P-S data acquisition include source type for optimal generation of converted waves and special recording cables with three-channel take-outs and simple connectors. More recent experience in 3-C acquisition is bringing costs down and improving quality.

Marine 4-C equipment and procedures are rapidly advancing as well. Topics of current attention include seafloor geophone coupling, the effects of geophone gimbaling, and receiver statics. For 3-D P-S wave data, shear waves can be polarized in any direction and it is therefore important that the response characteristics of the two horizontal geophones be identical. If their responses are different, data from the components cannot be combined optimally in a vector sense for 3-D processing.

Gaiser (1998) extends the concept of surface consistency to multicomponent receivers to correct for differences in geophone coupling between inline and crossline detectors from OBC data. Vector deconvolution operators are designed by minimizing transverse energy, and applied to inline and crossline data, resulting in multicomponent spectra that are well balanced. Figure 19 shows an example of portions of two crossline receiver gathers before and after compensation. It illustrates how undesirable 8 Hz resonance (Figure 19a) can be attenuated and the bandwidth of P-S wave reflections improved (Figure 19c). Correcting for variations in coupling helps the crossline component match the inline component for 3-D vector processing, and makes the crossline response more consistent for all receiver gathers.

### **P-S data processing**

As shown in Figure 1, the reflected S wave returns to the surface at a higher angle than the incident P wave. Thus, the reflection or conversion point is not midway between the source and receiver. Furthermore, this conversion-point location moves toward the receiver for shallower reflections and larger  $V_p/V_s$  values. Several authors have presented analysis of the asymmetric reflection point trajectory (Chung and Corrigan, 1985; Tessmer and Behle, 1988) and its importance in P-S imaging. Garotta (1985) outlined procedures for handling P-S data and presented additional interpretative uses for the data. Stewart (1991) extended Chung and Corrigan's (1985) work to describe converted waves where the source and receiver had unequal elevations.

Garotta et al. (1985), as mentioned previously, published one of the earliest papers on the analysis of P-S data. This insightful paper processed P-P and P-S data by handling vertical and horizontal channels separately with different statics and velocities. Also, the concept of what was later called, "asymptotic binning" was introduced. In asymptotic binning, the whole trace is put at the location defined by a reflector depth large compared to the source-receiver offset. For a single-layer case, this would be  $X_a = X/(1 + V_p/V_s)$ , where  $X_a$  is the conversion-point offset from the receiver position, and  $X$  is the source-receiver offset. Using one conversion point location avoids the complication of trace mapping prior to stack. They produced their final P-S sections using this gather and binning method.

Also, because of the low S velocity in the near-surface, receiver statics in the P-S survey can be large. Lawton (1990) gave numbers of about 70 ms for the receiver static for a case in the Alberta plains. Cary and Eaton (1993) found receiver statics of 100 ms. Isaac (1996) showed receiver statics of 100 ms in a case from Cold Lake, Alberta. The near-surface has a marked influence on P-S data as a result of large and variable statics. But, the near-surface has another undesirable effect: attenuation. This remains a limitation of surface P-S analysis. Further work on statics resolution, Q filtering, velocity analysis, and imaging will undoubtedly help.

Separation of P and S events on the full 3-C record has been approached using various techniques. In VSP analysis, methods based on Dankbaar's (1985) scheme of polarization analysis and  $f-k$  filtering have proven useful. Other work using 3-C array-

forming to reduce noise as well as to estimate direction and wave type looks promising. Yuan et al. (1998) show some excellent 4-C data from the North Sea, where they concluded that the P-S sections were of better quality than the P-P sections. They also used a matched-filter approach to remove P-S reflections from the vertical geophone data. Slotboom (1990) considered the velocity analysis problem. He derived a shifted hyperbola equation for NMO correction that can correct the offset travel-times better than a normal hyperbolic velocity analysis. Including a fourth-order term in the moveout equation can be helpful. Stewart and Ferguson (1996) presented a method to find a Dix S-wave interval velocity from P-S stacking velocities. Thomsen (1999) outlines a method of using an effective  $V_p/V_s$  value to better position events in a transversely isotropic medium.

After NMO, it is important to understand the Fresnel zone (or the averaging aperture in a stacked section) and the potential of P-S data to be migrated. Eaton et al. (1991) derived the P-S Fresnel zone and found that for the same frequencies, the P-S Fresnel radius is smaller than the corresponding P-P case. However, with the lower P-S frequencies often observed at the surface P-P and P-S radii work out to be about the same. They also showed that P-S data could be migrated post-stack in a kinematic sense. Harrison and Stewart (1993) considered the migration problem further and derived a P-S migration velocity for a horizontally layered material. As with P waves, P-S reflections are shifted in regions of dip. Thus, some procedures must be undertaken in the stacking process to put reflections at their correct zero-offset positions. Harrison (1992) developed an equation and procedure for the dip-moveout correction of converted-wave data. Several authors have investigated methods to enhance imaging via pre-stack migration (e.g. Nicholétis et al., 1998).

Carrying on with analysis of our reflectivity section, we may be interested in extracting an estimate of actual rock properties (e.g., impedance, velocity). Stewart (1991) derived a method for converting S-wave reflectivity to a shear-velocity log. This method is similar to seismic inversion via the Seislog® method. Cary (1994) details the processing flow for P-S waves in a 3-D survey. There is considerably more room in P-S analysis for enhancement of the data. Receiver statics remain a large problem as does adequate NMO-correction, and P-S imaging. The effects of anisotropy and multimode conversions can degrade the sections and are the subjects of current research.

### **Interpretation techniques**

As indicated earlier, Lawton and Howell (1992) developed a P-S synthetic seismogram program to assist in the correlation and interpretation process. This modelling algorithm uses the offset-dependent reflectivity and ray-traced traveltimes of both P-P and P-S waves to create synthetic seismograms. These seismograms are, in fact, AVO stacks of offset reflectivities. We can alter the  $V_p/V_s$  ratio in the P-P and P-S synthetic seismograms to tie P-P and P-S surface seismic sections. The zero-offset P-S reflection coefficient is zero, but the P-S section obviously does not attempt to provide this. Rather, the final P-S stack to zero-offset traveltimes gives an average of the offset-dependent P-S reflectivities.

Time structure sections and isochrons are used in P-S interpretation similarly to P-P techniques. However, we can also take the ratio of the P-P and P-S isochrons ( $T_{PP}$  and  $T_{PS}$ ) from the same interpreted horizons to generate  $V_p/V_s$  values. In this case,  $V_p/V_s = 2(T_{PS}/T_{PP}) - 1$ . Miller et al. (1998) show a case of this isochron-ratio analysis from the Lousana field, Alberta (Figure 20).

Finally, Larson (1996) develops interpretation techniques for the analysis of P-S data in 3-D geometry sections. Time slices, horizon maps, and various P-P and P-S ratio products are all useful. One 3C-3D seismic survey can provide three products: the P-P volume and the anisotropic volumes (P-S<sub>1</sub> and P-S<sub>2</sub>, where S<sub>1</sub> is the fast S wave and S<sub>2</sub> the slower S wave). Thus, there are a number of new, independent sections to compare, contrast, and integrate.

## CASE HISTORIES

### Lithology detection

Garotta et al. (1985) show P-S and P-P data for a Viking sand channel reservoir in the Winfield oil field, Alberta. They find amplitude anomalies on the P-S data correlating with the known boundaries of the reservoir. They also used isochron ratios to determine  $V_p/V_s$  and Poisson's ratios. They interpret low Poisson's ratios as differentiating sand from the neighbouring shales (Figure 21).

Nazar and Lawton (1993) used AVO stacks, P-P, and P-S sections to analyse the productive regions of the Carrot Creek field (Figure 22). The oil-saturated conglomerate in this region is not well imaged by conventional data but is apparent on P-S sections as a brightening in amplitude.

Miller et al. (1998) found significant variations in  $V_p/V_s$  in a carbonate play in Lousana, Alberta (Figure 20). The  $V_p/V_s$  values in the Cretaceous section (ranging from 2.2-2.5) are indicative of a clastic section while those in the Paleozoic (1.5-2.0) are characteristic of carbonate rocks. The lower values in the Paleozoic, from shot point 172 to 212, are coincident with an underlying oil-bearing reef. They interpret this anomaly as being associated with dolomitization.

Yang and Stewart (1996) reviewed a 9-C seismic survey from the Olds, Alberta area. This 10.3-km survey used vertical and horizontal vibrator sources along with 3-C geophones. The P-P section was of excellent quality, followed by a good P-S section, and a reasonable SH-SH section (Figure 23). The other components were fair to poor. They noted that there were  $V_p/V_s$  anomalies over a producing gas field that the line traversed.

A series of seismic experiments in the Blackfoot region of Alberta were conducted to identify sand reservoir facies from non-reservoir rocks. The surveys included broadband 3C-2D data, full 3C-3D data, 2-D and 3-D VSP surveys (Figure 24). The processed broad band 2-D lines tie reasonably well (Figure 25). Using this tie and picking isochrons, we can calculate an interval  $V_p/V_s$  value. We take an interval that includes the productive channel sand. There is a reasonable correlation of  $V_p/V_s$

anomalies and known oil production (Figure 26). The field was originally discovered and developed using P-wave amplitude anomalies (Figure 27); however, there are also false positives (amplitude anomalies) not associated with sand channels. P-P isochrons are also indicative of the channel but again not without some ambiguity. The P-S amplitude seems to give a more definitive (but lower resolution) image of the sand channel (Figure 28). A P-S isochron including the channel is perhaps more compelling (Figure 29). The  $V_p/V_s$  maps calculated from P-P and P-S isochron ratios are another strong indicator of the reservoir sand channel trend (Figure 30).

MacLeod et al. (1999a) show a case of converted waves successfully delineating sand channels encased in shale at the Alba field in the North Sea (Figure 31). A strong contrast in S-wave velocity is associated with the sand reservoir. Although P-wave velocity is sensitive to changes in fluid at the OWC, there is a relatively small contrast in P-wave velocity due to the change in lithology (Figure 31). A 4C OBC survey was conducted over Alba field to delineate the reservoir extent. Figure 32 illustrates the dramatically improved imaging of reservoir sands by P-S data relative to streamer P-wave data for a 2D section and a 3D view of the Alba field.

The impact of the 4C OBC survey on the development of Alba has been positive (MacLeod, et al., 1999b). To date, two successful wells have been drilled based primarily on the interpretation of the new converted-wave data. There are excellent ties between lithologies encountered in these wells and pseudo-elastic impedance computed from the converted-wave seismic response. Also, the P-S data have provided new insights into the complex geometry of the Alba field, suggesting significant post-depositional deformation of the turbidite channel.

### **Poor P-wave areas**

P-wave energy can be scattered and attenuated when passing through gas-saturated strata. Whether in the near-surface or just above the reservoir, gas-saturated sediments can seriously degrade imaging of deeper features.

Some areas in the North Sea have near-surface channels apparently containing biogenic gas that saturates poorly consolidated sediments (Figure 33). Although these hydrocarbon deposits are not economic, they are of interest because of their deleterious effect on conventional P-wave images. Reflections from interfaces within and below the gas-charged channels are extremely poor on the stacked P-wave section, exhibiting reverberations and attenuation of high frequencies. In contrast, the P-S section delineates the channel base, interfaces below the channel, and even sediment boundaries within the channel.

Leaky gas reservoirs can release a gas plume, which makes conventional imaging and characterization of the reservoir very difficult. S waves, on the other hand, are generally less sensitive to rock saturants and can be used to penetrate gas-saturated sediments as shown previously. The SUMIC (sub-sea seismic) technique used 3-C geophones planted on the ocean bottom (Berg et al., 1994). From these recordings, P-S images were constructed. Remarkable examples of this imaging through a gas chimney are shown in Figure 34 (Granli et al., 1995). Sections such as these have led

to an enormous interest in marine shooting with ocean-bottom cables (OBC) and sub-sea seismometers.

In cases where there are high-velocity layers – volcanics (e.g., basalts), carbonates, salts, or even permafrost in the near-surface, seismic imaging may be complicated or compromised. Purnell (1992) uses a physical model with a single high-velocity layer to demonstrate some of the modes that are observed in such a case. P waves convert to S waves with high efficiency going from low- to high-velocity layers. He finds that when migration is targeted to use these events (SPPS, SPPP, PPPS) some significantly improved images can be obtained.

### **Reservoir monitoring**

Isaac (1996) shows P-P and P-S sections from a heavy-oil reservoir at Cold Lake, Alberta that is undergoing steam flooding (Figure 35). There are changes in the reservoir rock properties associated with temperature and saturation changes. These, in turn, are associated with changes in the seismic character of both P-P and P-S sections. Using repeated surveys (Figure 36), she found that  $V_p/V_s$  could discriminate between hot, warm, and cold parts of the reservoir (Figure 37).

### **Structural imaging**

Resolution of steeply dipping features can be improved using converted waves in certain circumstances. Purnell (1992) shows examples from physical modelling data where high angle anomalies were more visible on migrated P-S data than migrated P-P data. High-velocity near-surfaces also have the potential to allow both P and S energy to propagate at angles away from the vertical. This puts the P-P and P-S energy on both vertical and radial channels.

Cary (pers. comm., 1999) shows examples from the Mahogany field in the Gulf of Mexico where P-S images show excellent definition of faults associated with salt intrusion. The P-wave section provides a better image deeper in the section. Improving P-S images at depth is a research challenge (Figure 38).

### **Anisotropy and fracture analysis**

Stewart et al. (1995) interpreted crossed P-S lines and VSP data from the Willesden Green area of Alberta. The survey was designed to find anisotropy (as an indicator of fracture) in the Second White Speckled shale. The time separation between the fast  $S_1$  and slow  $S_2$  shear wave may be related to fracture intensity, i.e. fracture density assumed proportional to the degree of azimuthal anisotropy. Fracture direction is then related to the orientation of the fast S-wave polarization. The data recorded were excellent and the tie between VSP and surface seismic was very good (Figure 39). But, there was no obvious anisotropy in the event times over 1.0 s to 3.0 s. However, the fractured shale is thin and further anisotropic analysis may reveal some fracture indicators. Ata and Michelena (1995) show an example of three 3-C seismic lines arranged in a star pattern in Venezuela. After processing and analysing

the data, they find indications of fracture direction from their calculated anisotropy (Figure 40).

Gaiser (1999) shows analyses of a full 3C-3D seismic survey from the Madden field in the Wind River Basin, Wyoming. This analyses uses 4-component Alford (1986) rotations and layer stripping (Winterstein and Meadows, 1991a) to calculate the fast shear-wave ( $P-S_1$ ) polarization direction and the associated percent anisotropy. Figure 41 is a portion of the data from an east-west line: the radial and transverse polarization for east-west propagation. There are equivalent sections for north-south propagation. To compensate for the effects of depth varying properties (Winterstein and Meadows, 1999b), the reflection at 1.5 s is analysed first to remove shear-wave splitting effects from the overburden. Although the energy on the transverse component for this event is weak in places, removing overburden effects from the target reflections below is an important step to unravel shear-wave birefringence. Figure 42 shows the fast S-wave direction and its associated percent anisotropy, corresponding to possible fracture orientation and fracture density of the target horizons between 2.2 and 3.3 s. Regions of high percent anisotropy (9% or more) correlate well with the known east-west trending faults superimposed on the maps.

As in many situations there is an issue of resolution. These fracture property estimates are an average over 1.1 seconds of data, an interval clearly larger than the reservoirs of interest. Fracture detection at finer intervals can be attempted by careful survey design, providing optimal fold, offset and azimuthal distribution.

Numerical modelling (Li et al., 1996) suggests that gas-saturated oriented fractures may have a distinct effect on P-S velocity (Figure 43). This is in contrast to conventional isotropic thinking, where fluid saturation has little impact on S-wave velocities. Guest et al. (1998) interpret anomalies in S-wave splitting over a gas reservoir in Oman as evidence of an effect of gas on shear waves.

## **WHAT'S LEFT TO DO**

Converted-wave exploration has come a long way in the last several years. But, there's still a lot of room left for progress.

Determining which recording environments allow acquisition of good P-S data and how to carry out that acquisition is an area for further effort. Much remains to be done in designing ocean-bottom recording systems. Moldoveanu et al. (1998) indicate that even in transition zones P-S data can be acquired by ramming 4-C receivers into the mud. New solid-state, digital geophones (and newer optical motion sensors) with three and four components promise more complete recordings (even close to 0 Hz).

Investigating other modes in multicomponent data will allow us to separate undesirable from desirable modes as well as to make other sections. In some cases, a vertical vibrator may also generate enough S-wave energy to allow an S-S section to be created directly. And, of course, if the signal is there we should try to use it. Fyfe et al. (1993) show a case from Saudi Arabia in which good P-S and S-S sections were

produced from a vertical vibrator source recorded into 3-C geophones. Furthermore, an S-S section may be produced from dynamite data. Nieuwland et al. (1994) give an example of processing a P-S-S survey in the Netherlands. In this case, an upgoing P wave from the dynamite source converts at the surface to a downgoing S wave that is reflected back to the surface from various layers as an S wave. Credible S-wave sections are produced, along with their P-wave counterparts, and are interpreted for gas effects. A P-S-S event may be extractable from marine 4-C data in some cases.

Another multipathing event is a P wave converting to an S wave reflecting as an S event, then converting back to a P wave. This energy, a PS-SP event may be imaged on conventional data by using an S-wave velocity for a region in the migration. The base of high velocity layers (HVL) can be effectively imaged using mode-converted S waves by replacing the P-wave velocity in the HVL with an appropriate S-wave velocity (Purnell, 1992). Figure 44 illustrates this approach with streamer data where an S-wave velocity structure for the salt body has been derived and used in a PSSP depth migration. The result is that shear-wave multimodes (in this case base of salt) tend to map to comparable P-wave structures. Although conversion back to P wave at the top of HVLs is not required for land acquisition, it is for marine acquisition because S waves can not propagate through water to streamer hydrophones.

More sophisticated processing techniques will be useful to estimate statics, identify and use anisotropy, estimate velocities, and do accurate migrations. We also need to understand a great deal more about how the near-surface damages S-wave data.

There are many areas of poor data recording such as the Michigan Basin, Rocky Mountain Foothills, northern Ireland and carbonate outcrops in the Middle East. We are challenged to understand why these areas are no-record (NR) and what we can do about them. P-S imaging in complex structural environments may produce credible images.

## **CONCLUSIONS**

The reflection seismic method has used P waves for many years – and with great success. However, there is more to be done in exploration seismology, especially by using the other elastic modes that are part of the seismic survey (particularly the P-S waves).

P-S seismic exploration has been developing for about 15 years. There are currently commercial design, acquisition, processing and interpretation groups. Many new examples show successful cases of P-S imaging and hydrocarbon related interpretation.

## **ACKNOWLEDGMENTS**

We would like to express our deep appreciation to the sponsors of the CREWES Project for their commitment to the development of multicomponent seismology.

Many thanks to CREWES staff Chuandong Xu, Henry Bland, and Louise Forgues for help in assembling this paper.

The authors express their gratitude to Neil Jones, Rich Van Dok and Robert Bloor of Western Geophysical Co. for providing data examples and to Heloise Lynn for her insightful interpretations of the 3C Madden survey. We thank the Alba partnership (Chevron, Arco, Conoco, Fina, Petrobras, Saga, Statoil and Unilon/Baytrust) for their permission to include the Alba data, and in particular Mark MacLeod of Chevron UK Ltd. for his efforts in supplying the Alba examples.

## REFERENCES AND FURTHER READING

- Aki, K. and Richards, P.G., 1980, Quantitative seismology: Theory and methods: W.H. Freeman and Sons, vols 1 and 2.
- Alford, R.M., 1986, Shear data in the presence of azimuthal anisotropy: Dilly, Texas, 56th Ann. Intl. SEG Meeting, Expanded Abstracts, S9.6, 476-479.
- Arnold, A. and Chiburis, E., 1998, AVO – Current status and the future: Presented at 68th Ann. Intl. SEG Meeting, Expanded Abstracts, 248-250.
- Ata, E. and Michelena, R.J., 1995, Mapping distribution of fractures in a reservoir with P-S converted waves: The Leading Edge, 664-676.
- Ata, E., Michelena, R.J., Gonzales, M., Cerquone, H., and Carry, M., 1994, Exploiting P-S converted waves: Part 2, Application to a fractured reservoir: 64th Ann. Intl. SEG Meeting, Expanded Abstracts, 240-243.
- Behle, A. and Dohr, G.P., 1985, Converted waves in exploration seismics: in Dohr, G.P., ed., Seismic shear waves: Part B: Applications: Geophysical Press, v. 15B.
- Berg, E., Svenning, B., and Martin, J., 1994, SUMIC: Multicomponent sea-bottom seismic surveying in the North Sea – Data interpretation and applications: 64th Ann. Intl. SEG Meeting, Expanded Abstracts, 477-480.
- Campbell, A., Percy, R., Lee, H., and Hemingson, P., 1994, Judy Creek: Successful use of offset VSP to find porosity: 64th Ann. Intl. SEG Meeting, Expanded Abstracts, 115-120.
- Cary, P.W., 1994, 3C-3D converted-wave seismic: CREWES Research Report, 5, 31.1-31.10.
- Cary, P.W. and Eaton, D.W.S., 1993, A simple method for resolving large converted-wave (P-SV) statics: Geophysics, 58, 429-433.
- Cary, P.W., Pye, G., and Harrison, M.P., 1993, Shear-wave splitting analysis with converted waves: New processing techniques: Ann. Nat. Meeting, Can Soc. Expl. Geophys., Abstracts, 72-74.
- Chung, W.Y. and Corrigan, D., 1985, Gathering mode-converted shear waves: A model study: 55th Ann. Intl. SEG Meeting, Expanded Abstracts, 602-604.
- Coulombe, C.A., Stewart, R.R., and Jones, M.E., 1996, AVO processing and interpretation of VSP data: Can. J. Expl. Geophys., 32, 1, 41-62.
- Dankbaar, J.W.M., 1985, Separation of P- and S-waves: Geophys. Prosp., 33, 970-986.
- Donati, M.S. and Brown, R.J., 1995, Birefringence study on 3-C/2-D: Barinas Basin (Venezuela): Exp. Abst., 65th Ann. Intl. Meeting, Soc. Expl. Geophys., 723-726.
- Donati, M.S. and Stewart, R.R., 1996, P- and S-wave separation at a liquid-solid interface: J. Seis. Explor., 5, 113-127.
- Eaton, D.W.S. and Lawton, D.C., 1992, P-SV stacking charts and binning periodicity: Geophysics, 57, 745-748.
- Eaton, D.W.S., Stewart, R.R., and Harrison, M.P., 1991, The Fresnel zone for P-SV waves: Geophysics, 56, 360-364.
- Frasier, C. and Winterstein, D., 1990, Analysis of conventional and converted mode reflections at Putah Sink, California using three-component data: Geophysics, 55, 646-659.
- Fyfe, D.J., Dent, B.E., Kelamis, P.B., Al-Mashouq, K.H., and Nietupski, D.A., 1993, Three-component seismic experiments in Saudi Arabia: 55th Ann. Meeting Europ. Assn. Expl. Geophys.
- Gaiser, J.E., Fowler, P.J., and Jackson, A.R., 1997, Challenges for 3-D converted-wave processing, 67th Ann. Intl. SEG Meeting, Expanded Abstracts, SP5.2, 1199-1202.

- Gaiser, J.E., 1998, Compensating OBC data for variations in geophone coupling, 68th Ann. Intl. SEG Meeting, Expanded Abstracts, SP 12.6, 1429-1432.
- Gaiser, J.E., 1999, Applications for vector coordinate systems of converted waves obtained by multicomponent 3-D data, 31st Ann. Off. Tech. Conf., Houston, OTC 10985.
- Garotta, R., 1985, Observation of shear waves and correlation with P events: in Dohr, G.P., ed., Seismic shear waves: Part B: Applications: Geophysical Press, v. 15B.
- Garotta, R., Marechal, P., and Magesan, M., 1985, Two-component acquisition as a routine procedure for recording P-waves and converted waves: Can. J. Expl. Geophys., 21, 40-53.
- Geis, W.T., Stewart, R.R., Jones, M.J., and Katopodis, P.E., 1990, Processing, correlating, and interpreting converted shear waves from borehole data in southern Alberta: Geophysics, 55, 660-669.
- Goodway, W., Chen, T., and Downton, J., 1997, Improved AVO fluid detection and lithology discrimination using Lamé petrophysical parameters: *lr*, *mr*, and *l/m* fluid stack, from P and S inversions: Presented at CSEG Ann. Nat. Meeting.
- Granli, J.R., Sollid, A., Hilde, E., and Arnsten, B., 1995, Imaging through gas-filled sediments with marine S-wave data: 65th Ann. Intl. SEG Meeting, Expanded Abstracts.
- Guest, S., Vander Kolk, C., and Potters, H., 1998, The effect of fracture filling fluids on shear-wave propagation: 68th Ann. Intl. SEG Meeting, Expanded Abstracts, 948-951.
- Harrison, M.P., 1992, Processing of P-SV surface-seismic data: Anisotropy analysis, dip moveout, and migration: Ph. D. thesis, The University of Calgary.
- Harrison, M.P. and Stewart, R.R., 1993, Post-stack migration of P-SV seismic data: Geophysics, 58, 1127-1135.
- Hoffe, B.H., Bland, H.C., Margrave, G.F., Manning, P.M., and Foltinek, D.S., 1999, Analysis of the effectiveness of 3-C receiver arrays for converted wave imaging: Ann. Intl. SEG Meeting, Expanded Abstracts, SAC02.7.
- Isaac, J., 1996, Seismic methods for heavy oil reservoir monitoring: Ph.D. thesis, The Univ. of Calgary.
- Kendall, R.R. and Davis, T.L., 1996, The cost of acquiring shear waves: The Leading Edge, 15, 8, 943-949.
- Kendall, R.R., Gray, S.H., and Murphy, G.E., 1998, Subsalt imaging using prestack depth migration of converted waves: Mahogany Field, Gulf of Mexico: 68th Ann. Intl. SEG Meeting, Expanded Abstracts, 2052-2055.
- Larson, G.A. 1996, Acquisition, processing, and interpretation of P-P and P-S 3-D seismic data: M.Sc. thesis, The University of Calgary.
- Lawton, D.C., 1990, A 9-component refraction seismic experiment: Can. J. Expl. Geophys., 26, 7-16.
- Lawton, D.C. and Harrison, M.P., 1992, A two-component reflection seismic survey, Springbank, Alberta: Can. J. Expl. Geophys., 28, 30-43.
- Lawton, D.C. and Howell, C.T., 1992, P-SV and P-P synthetic stacks: 62nd Ann. Intl. SEG Meeting, Expanded Abstracts, 1344-1347.
- Lawton, D.C. and Bertram, M.B., 1993, Field tests of 3-component geophones: Can. J. Expl. Geophys., 29, 125-131.
- Lawton, D.C., Stewart, R.R., Cordsen, A., and Hrycak, S., 1995, Advances in 3C-3D design for converted waves: CREWES Research Report, 7, 43.1-43.41.
- Li, X., Kuhnel, T., and MacBeth, C., 1996, Converted-wave AVO and its implications: Extd. Abst., 58th Ann. Intl. Meeting, Europ. Assn. Geosci. Eng., M046.
- MacLeod, M.K., Hadley, M.J., Reynolds, K.J., and Tura, A., 1999a, Multicomponent analysis of OBC data, 31st Ann. Off. Tech. Conf., Houston, OTC 10940.
- MacLeod, M.K., Hanson, R.A., Bell, C.R., and McHugo, S., 1999b, The Alba field ocean bottom cable seismic survey: Impact on development, Off. Euro. Conf., Aberdeen, SPE 56977.
- Mari, J.L., Coppens, F., Gavin, P., and Wicquart, E., 1994, Full waveform acoustic data processing: Editions Technip.
- Michelena, R.J., Ata, E., and Sierra, J., 1994, Exploiting P-S converted waves: Part 1, Modelling the effects of anisotropy and heterogeneities: 64th Ann. Intl. SEG Meeting, Expanded Abstracts, 236-239.
- Michelena, R.J., 1995, Quantifying errors in fracture orientation estimated from surface P-S converted waves: 65th Ann. Intl. SEG Meeting, Expanded Abstracts, 282-285.

- Miller, S.L.M., 1992, Well log analysis of  $V_p$  and  $V_s$  in carbonates: CREWES Research Report, 4, 12.1-12.11.
- Miller, S.L.M., 1996, Multicomponent seismic data interpretation: M.Sc. thesis, University of Calgary.
- Miller, S.L.M. and Stewart, R.R., 1990, The effect of lithology, porosity and shaliness on P- and S-wave velocities from sonic logs: *Can J. Expl. Geophys.*, 26, 94-103.
- Miller, S.L.M., Harrison, M.P., Szata, K.J., Stewart, R.R., and Lawton, D.C., 1998, Interpretation of a carbonate reservoir using P-P and P-SV seismic data: Submitted to *Geophysics*.
- Moldoveanu, N., Rink, U., and Van Baaren, P., 1998, Multicomponent acquisition in transition zone environment: an experimental study: 68th Ann. Intl. SEG Meeting, Expanded Abstracts, 738-739.
- Nicholétis, L., Svay-Lucas, J., and Prigent, H., 1998, True amplitude pre-stack imaging of converted waves: 68th Ann. Intl. SEG Meeting, Expanded Abstracts, 734-737.
- Nazar, B.D. and Lawton, D.C., 1993, AVO analysis of a thin conglomerate deposit: *J. Seis. Expl.*, 2, 333-348.
- Nieuwland, F., Marschall, R., Papaterpos, M., and Sharp, D., 1994, An example of the use of shear waves in seismic exploration: *J. Seis. Explor.*, 3, 5-20.
- Purnell, G.W., 1992, Imaging beneath a high-velocity layer using converted waves: *Geophysics*, 57, 1444-1452.
- Slotboom, R.T., 1990, Converted wave (P-SV) moveout estimation: 60th Ann. Intl. SEG Meeting, Expanded Abstracts, 1104-1106.
- Stewart, R.R., 1991, Rapid map and inversion of P-SV waves: *Geophysics*, 56, 859-862.
- Stewart, R.R. and Ferguson, R., 1993, S-wave interval velocity from P-S stacking velocity: *Geophysics*, 58, 1127-1135.
- Stewart, R.R., Pye, G., Cary, P.W., and Miller, S.L.M., 1995, Interpretation of P-SV seismic data: Willesden Green, Alberta: CREWES Research Report, 5, 15.1-15.19.
- Stewart, R.R., Ferguson, R., Miller, S.L.M., Gallant, E., Margrave, G., 1996, The Blackfoot seismic experiments: Broad-band, 3C-3D, and 3-D VSP surveys: *CSEG Recorder*, 6, 7-10.
- Tatham, R.T., 1982,  $V_p/V_s$  and lithology: *Geophysics*, 47, 336-344.
- Tessmer, G. and Behle, A., 1988, Common reflection point data stacking technique for converted waves: *Geophys. Prosp.*, 36, 671-688.
- Thomsen, L., 1999, Converted-wave reflection seismology over inhomogeneous anisotropic media: *Geophysics*, 64, 678-690.
- Van Dok, R.R., Gaiser, J.E., Jackson, A.R., and Lynn, H.B., 1997, 3-D converted-wave processing: Wind River Basin case history, 67th Ann. Intl. SEG Meeting, Expanded Abstracts, SP5.4, 1206-1209.
- Winterstein, D.F. and Meadows, M.A., 1991a, Shear-wave polarizations and subsurface stress directions at Lost Hills field, *Geophysics*, 56, 1331-1348.
- Winterstein, D.F. and Meadows, M.A., 1991b, Changes in shear-wave polarization azimuth with depth in Cymric and Railroad Gap oil fields, *Geophysics*, 56, 1349-1364.
- Xu, P. and Parra, J.O., 1998, A parametric study of synthetic dipole logging data in azimuthally anisotropic formations: 68th Ann. Intl. SEG Meeting, Expanded Abstracts, 260-263.
- Yang, G. and Stewart, R.R., 1996, A 9-C seismic survey: Olds, Alberta, CREWES Research Report, 8.
- Yuan, J., Li, X., Ziolkowski, A., and Strijbos, F., 1998, Processing 4-C sea floor seismic data: a case example from the North Sea: 68th Ann. Intl. SEG Meeting, Expanded Abstracts, 714-717.

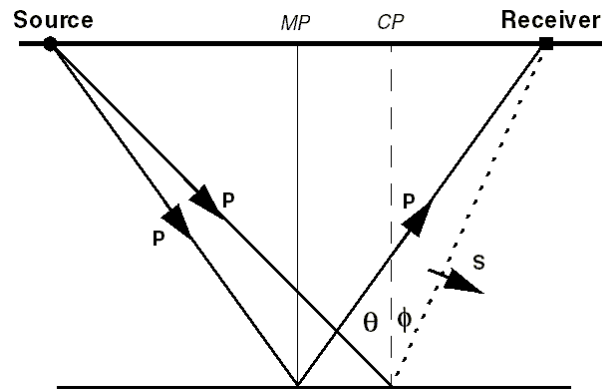


Fig. 1: A converted-wave (P-S) reflection at its conversion point (*CP*) compared to a pure P-wave reflection at its midpoint (*MP*). Note that *CP* is shifted toward the receiver. The P-wave incidence angle is given by  $\theta$  and S-wave reflection angle by  $\phi$ . Arrows show the senses of positive phase or of first motion when the two reflection coefficients are both positive (after Aki and Richards, 1980, p 139). Note that the P-P and P-S reflection coefficients are normally, but not always, of *opposite* sign (see e.g. Brown, 1999).

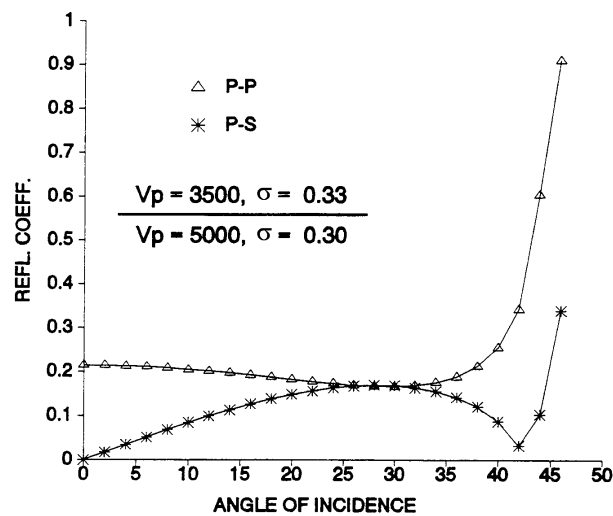


Fig. 2: P-P and P-S reflection coefficients as functions of P-wave angle of incidence for a clastic-over-carbonate example. Note that we have plotted the absolute values for the P-S reflection, its phase being at  $180^\circ$  (opposite) to that of the P wave in this, but not all, cases. The density values are 2400 and 2500  $\text{kg/m}^3$  and the given values of  $V_p$  and  $\sigma$  (Poisson's ratio) correspond to  $V_s$  values of 1763 and 2673 m/s above and below, respectively.

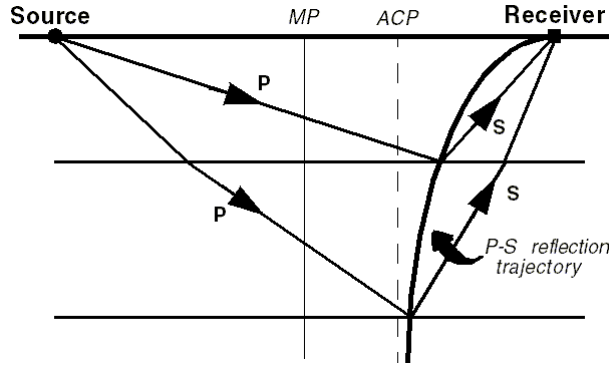


Fig. 3: The P-S conversion point locus with its asymptotic conversion point (ACP) at large depth.

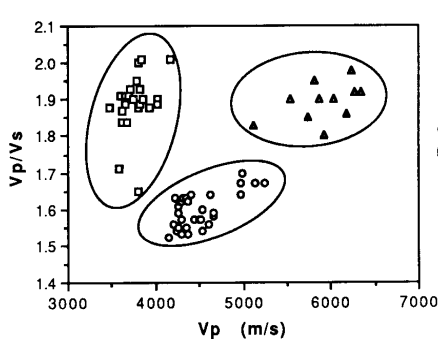


Fig. 4(a): Well log  $V_p/V_s$  values versus  $V_p$  for pure and mixed lithologies of the Medicine River field (from Miller and Stewart, 1990).

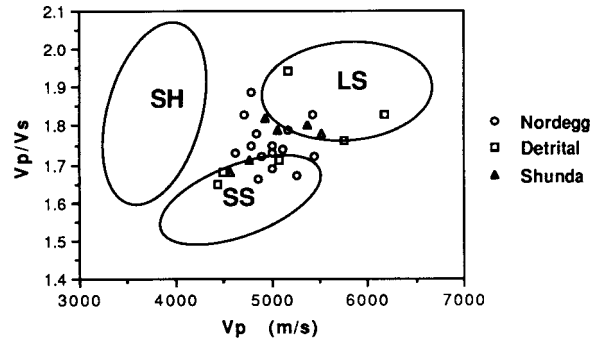


Fig. 4(b):  $V_p/V_s$  value versus  $V_p$  for mixed lithologies (from Miller and Stewart, 1990).

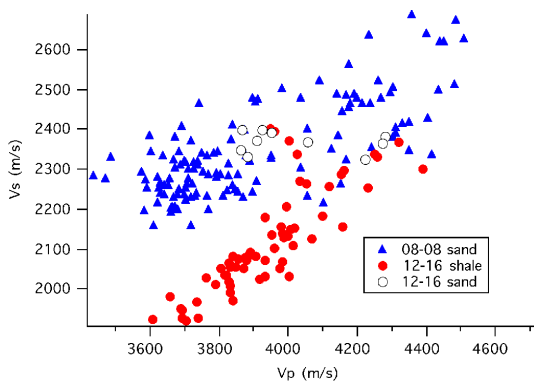


Fig. 5(a):  $V_s$  versus  $V_p$  values from well logs for a sand reservoir and off-reservoir shale.  $V_s$  is significantly higher in sand than shale in these wells (Miller, 1996).

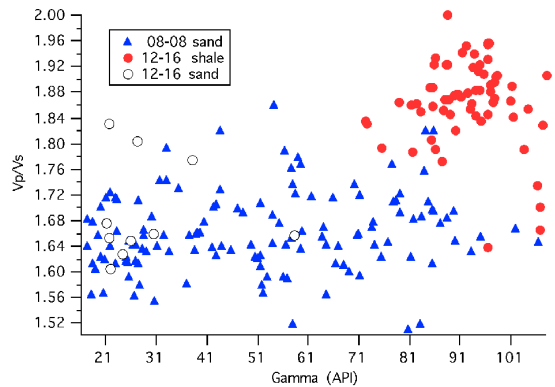


Fig. 5(b):  $V_p/V_s$  value versus gamma value from well logs as in 4(a).  $V_p/V_s$  has slight increase with shaliness in sand. More pure shales have distinctly higher  $V_p/V_s$  values.

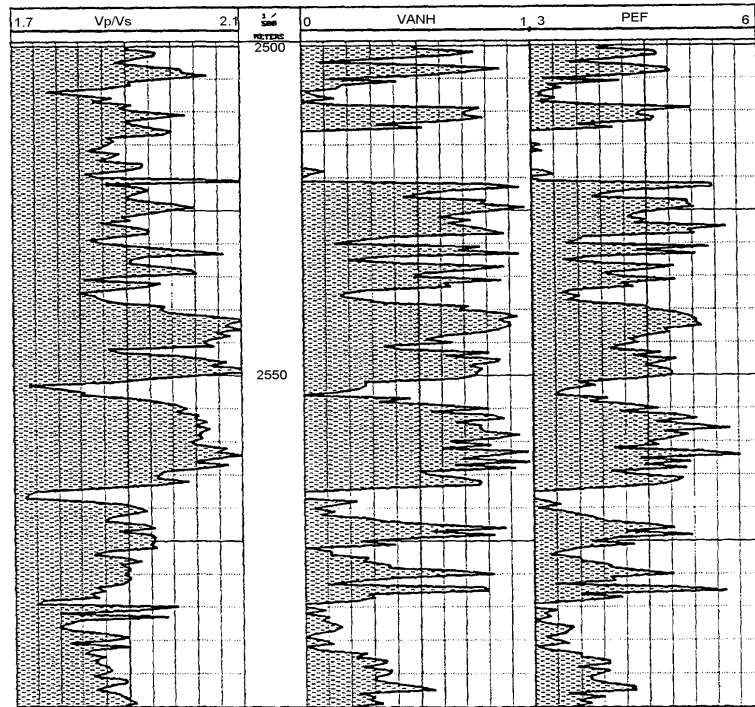


Fig. 6:  $V_p/V_s$ , volume anhydrite (versus dolomite), and photoelectric logs plotted in depth for the Davey well (from Miller, 1992). Note the consistent tracking of  $V_p/V_s$  with the anhydrite volume.

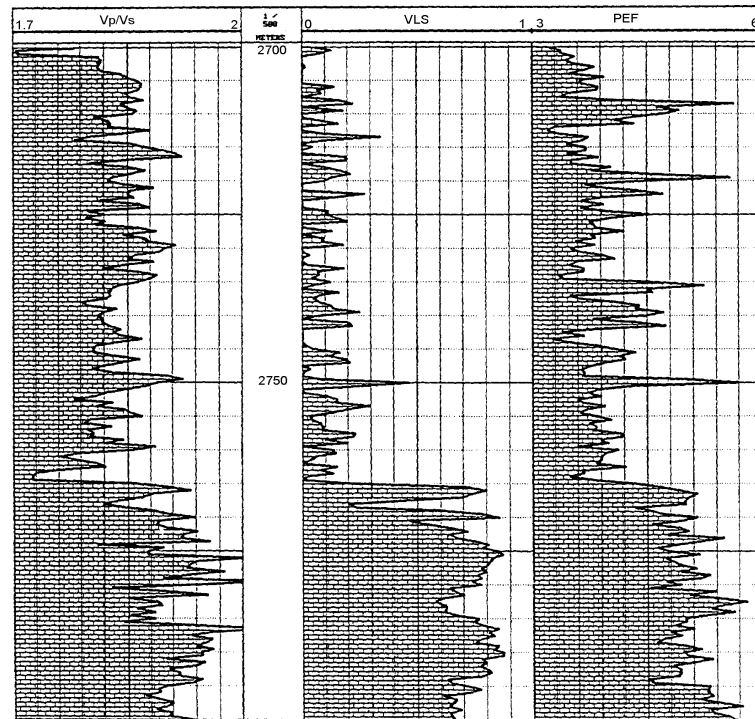


Fig. 7:  $V_p/V_s$ , volume limestone (versus dolomite), and photoelectric logs plotted in depth for the Davey well. Note the consistent tracking of  $V_p/V_s$  with the limestone volume (from Miller, 1992).

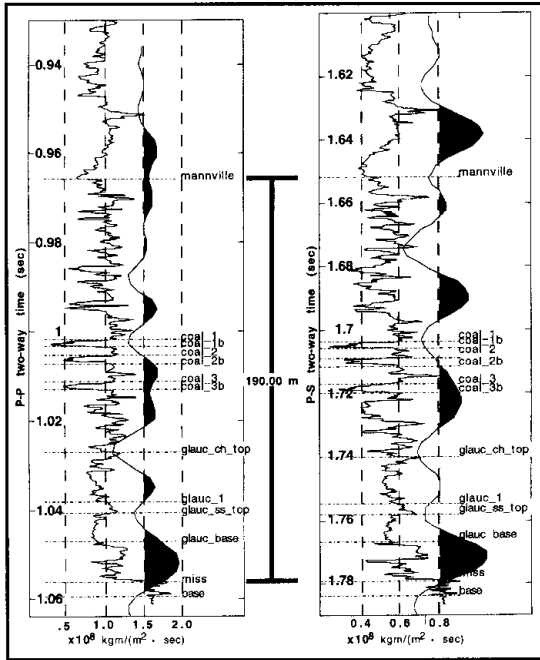


Fig. 8: P-wave impedance log and P-P synthetic seismogram and S-wave impedance log and corresponding P-S synthetic seismogram for the 08-08-23-23W4 well in the Blackfoot field, southern Alberta (from Stewart et al., 1996).

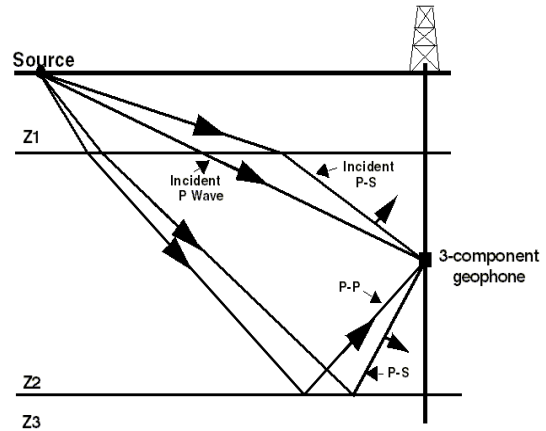


Fig. 9: VSP geometry with an offset source. Both transmitted and reflected P-P and P-S waves are shown.

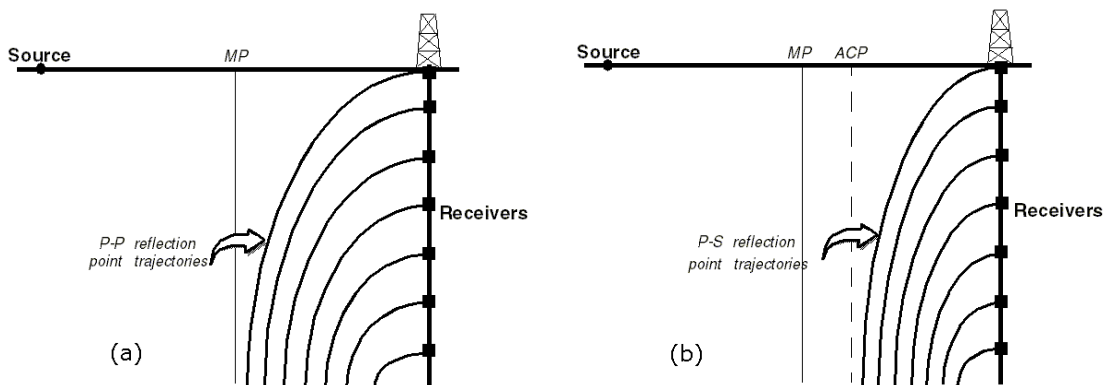


Fig. 10: Schematic diagram of a) P-P reflection trajectories and b) P-S conversion points for the VSP case.

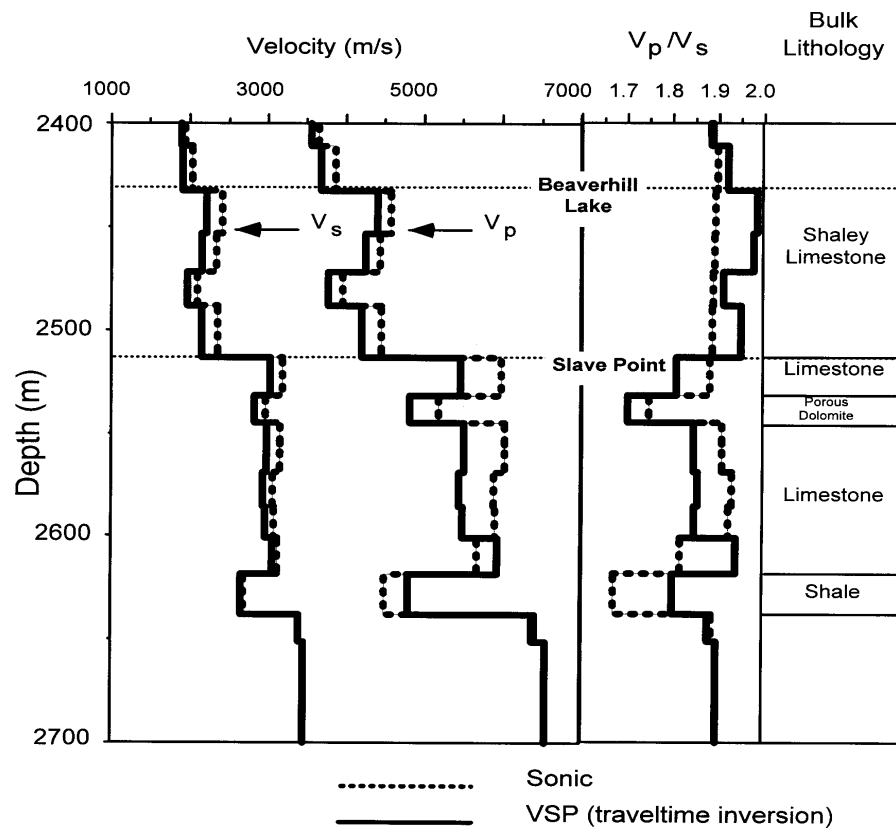


Fig. 11: Interval velocity from VSP and blocked sonic logs. The porous dolomite reservoir shows a significant  $V_p/V_s$  drop relative to surrounding limestones (from Coulombe et al., 1996).

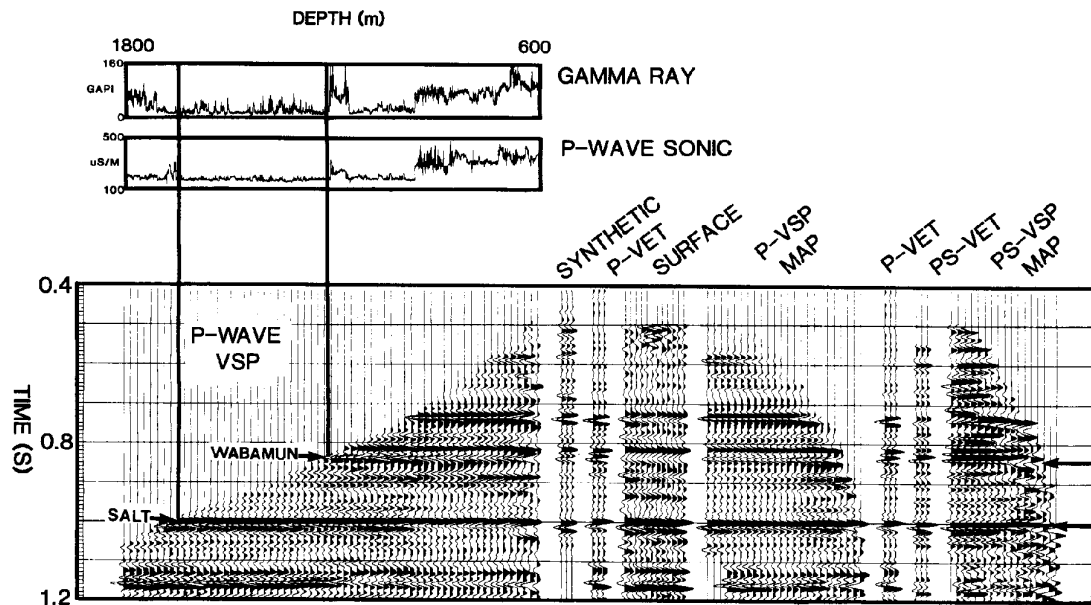


Fig. 12: Composite plot showing well logs in depth, the VSP in depth and two-way traveltime, synthetic seismograms, P-wave surface seismic, and VSP sections. Data are from S. Alberta. Note the great reflection activity (and noise) in the converted-wave section (from Geis et al., 1990).

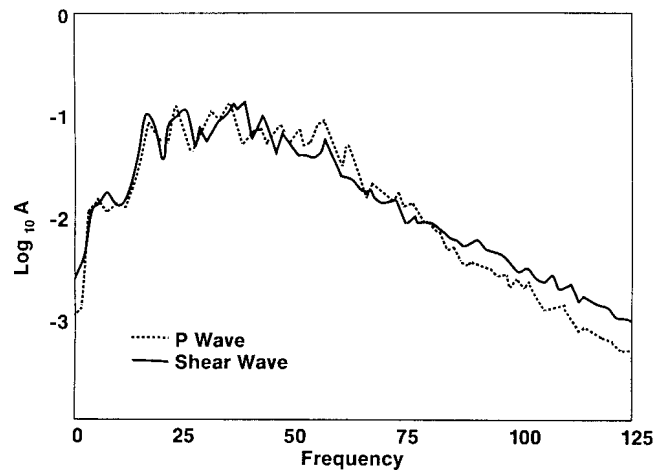


Fig. 13: Spectra from the P-wave VSP and P-S VSP data. The same temporal frequency of P-wave and S-wave data indicates a higher spatial resolution of the S-wave data (from Geis et al., 1990).

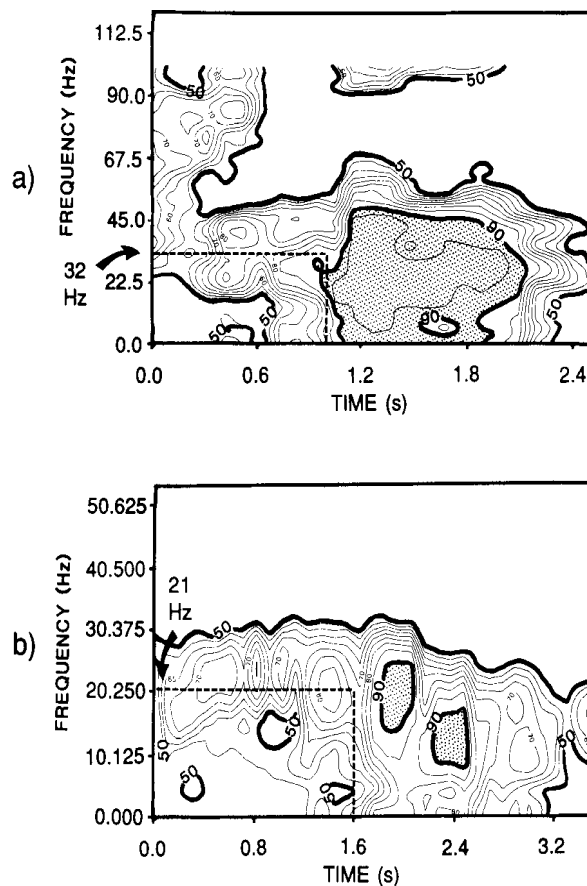


Fig. 14: Frequency coherency spectra from the Carrot Creek, Alberta surveys (a) P-P data and (b) P-S data. At the depth of interest, the P-P dominant frequency is 32 Hz and the P-S value is 21 Hz (from Eaton et al., 1991)

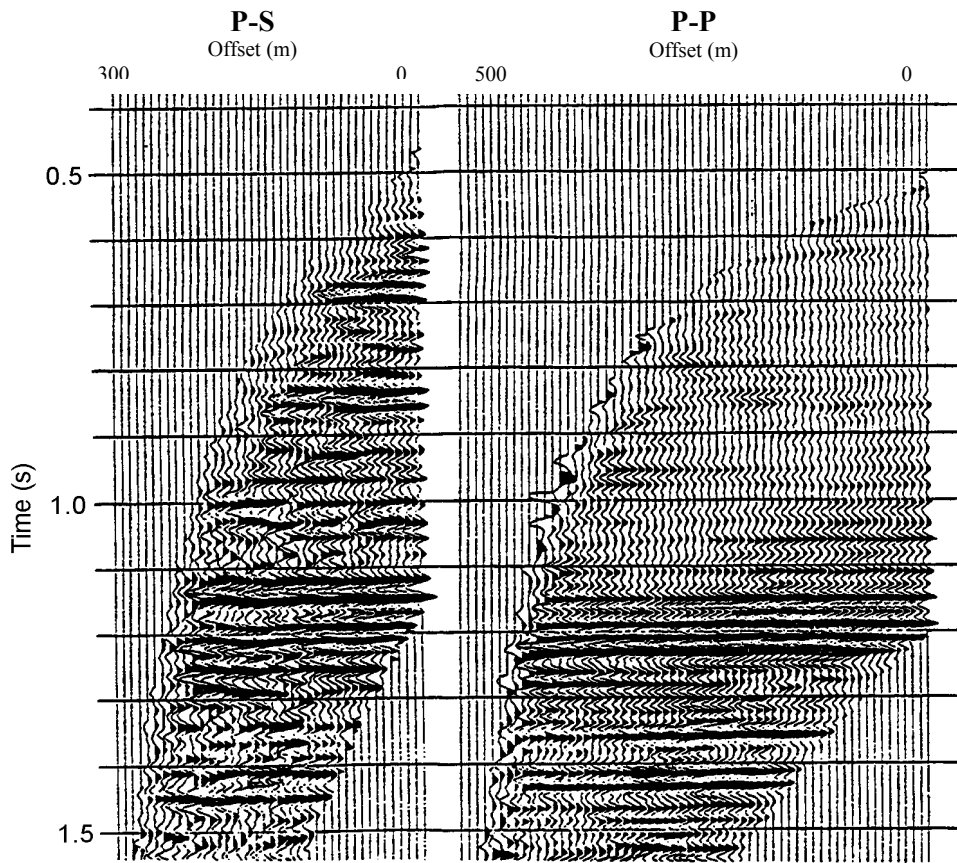


Fig. 15: P-S and P-P VSP sections from the Willesden Green surveys (Stewart et al., 1995). Note the greater reflection activity in the P-S section in the shallow regions.

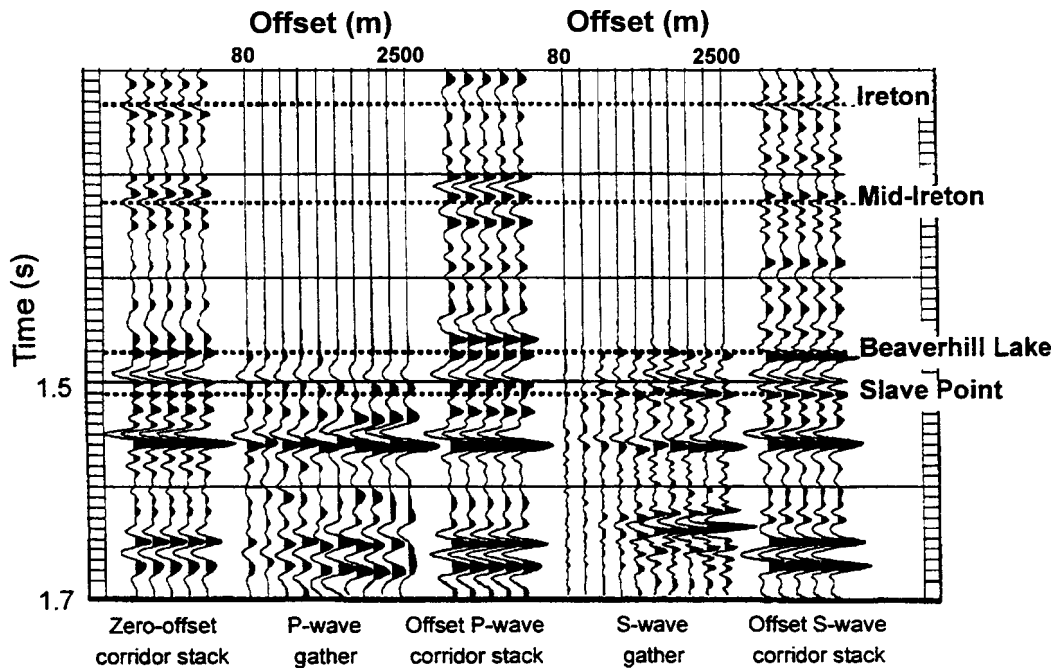


Fig. 16: Amplitude versus offset traces for VSP data. The P-wave and S-wave gathers are from offsets ranging from 80m to 2500m (from Coulombe et al., 1996).

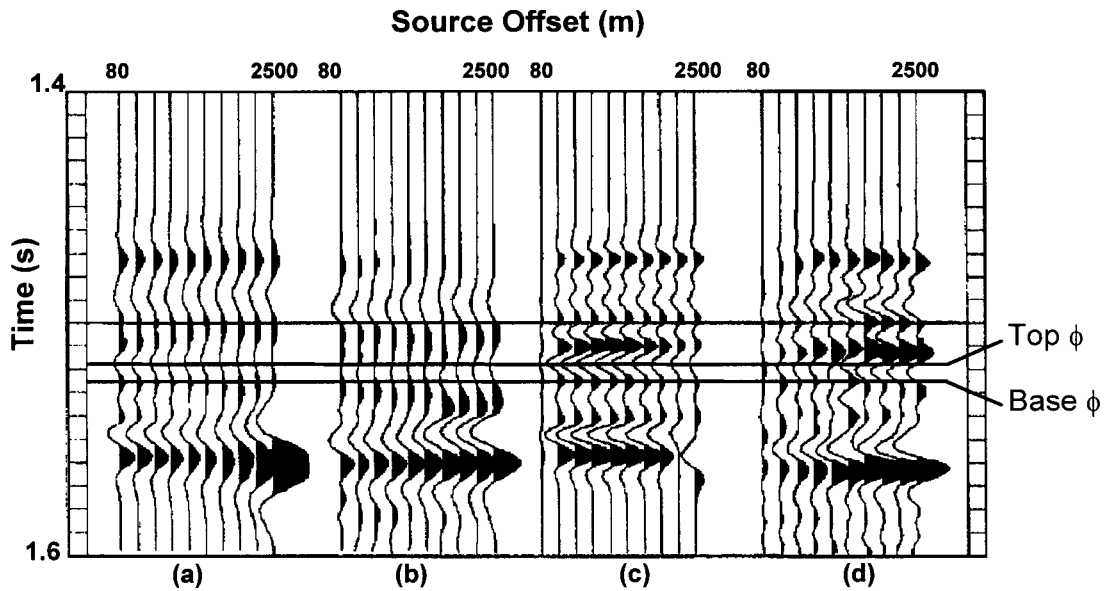


Fig. 17: Amplitude versus offset traces for VSP data. The P-wave modelled synthetic (a) and field data (b) show AVO effects as do the P-S data – synthetic (c) and field (d). The gathers are from source offsets ranging from 80m to 2500m (from Coulombe et al., 1996). The top and bottom of the interpreted porous dolomite layer are indicated.

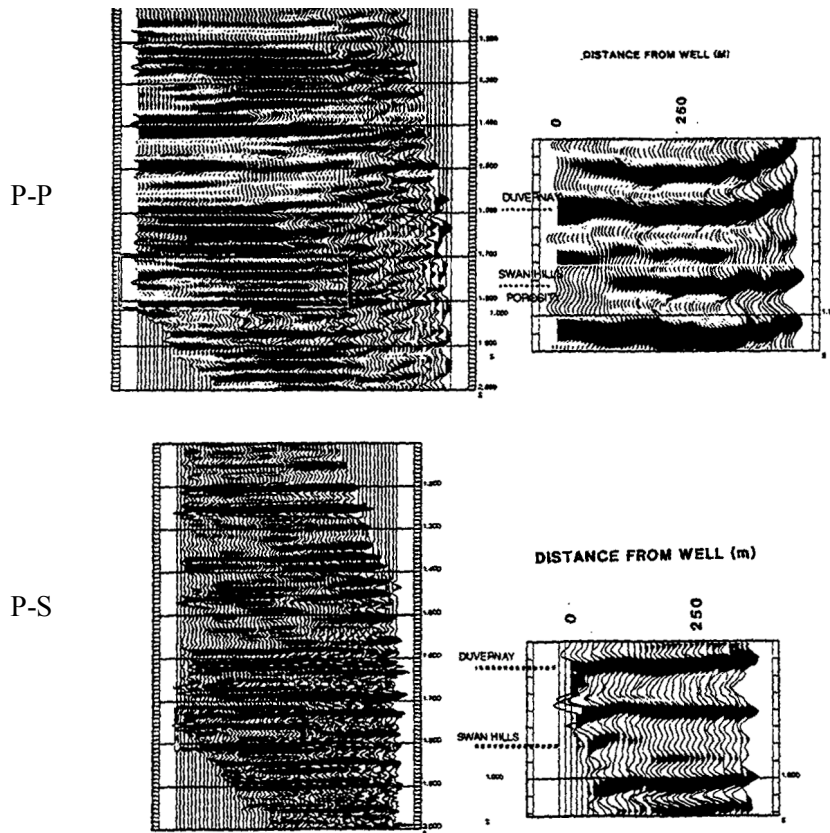


Fig. 18: P-wave and P-S images from the Judy Creek, Alberta VSP surveys. Both images indicated a porosity anomaly beginning about 125 m from the well location (from Campbell et al., 1994).

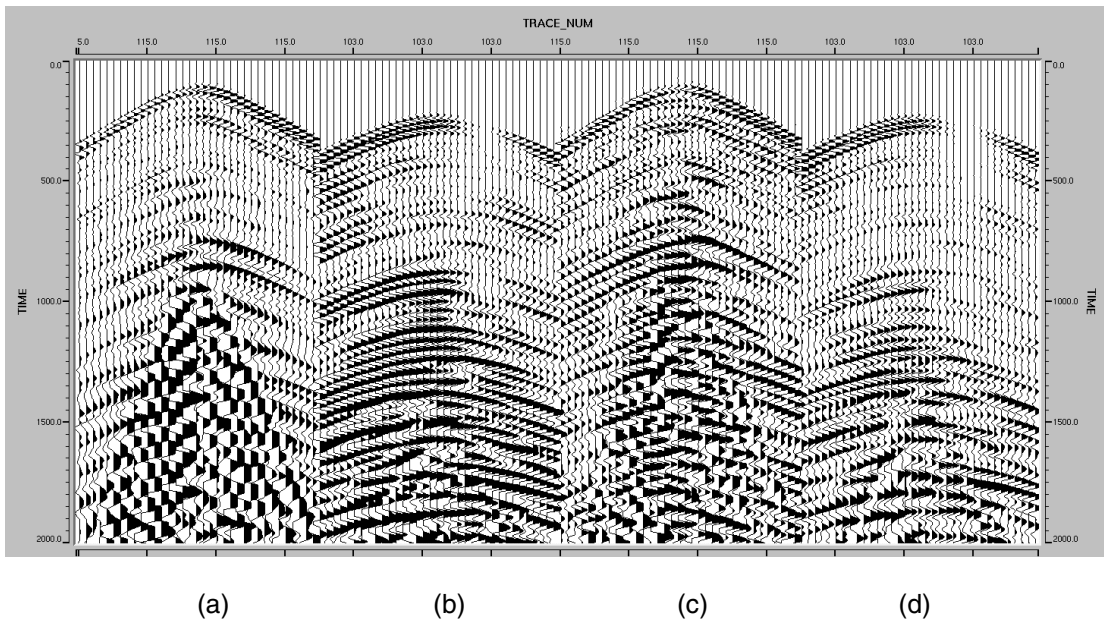


Fig. 19: Crossline responses from portions of two different 3-D common-receiver gathers before compensation (a) and (b), and after compensation (c) and (d). Gather (a) is an example of a poorly coupled receiver exhibiting 8 Hz resonance, and gather (b) is an example from an average coupled receiver. After correction the two receiver gathers are better balanced in their frequency content, indicated by bandwidth, and relative amplitudes of reflections and sediment-water interface waves.

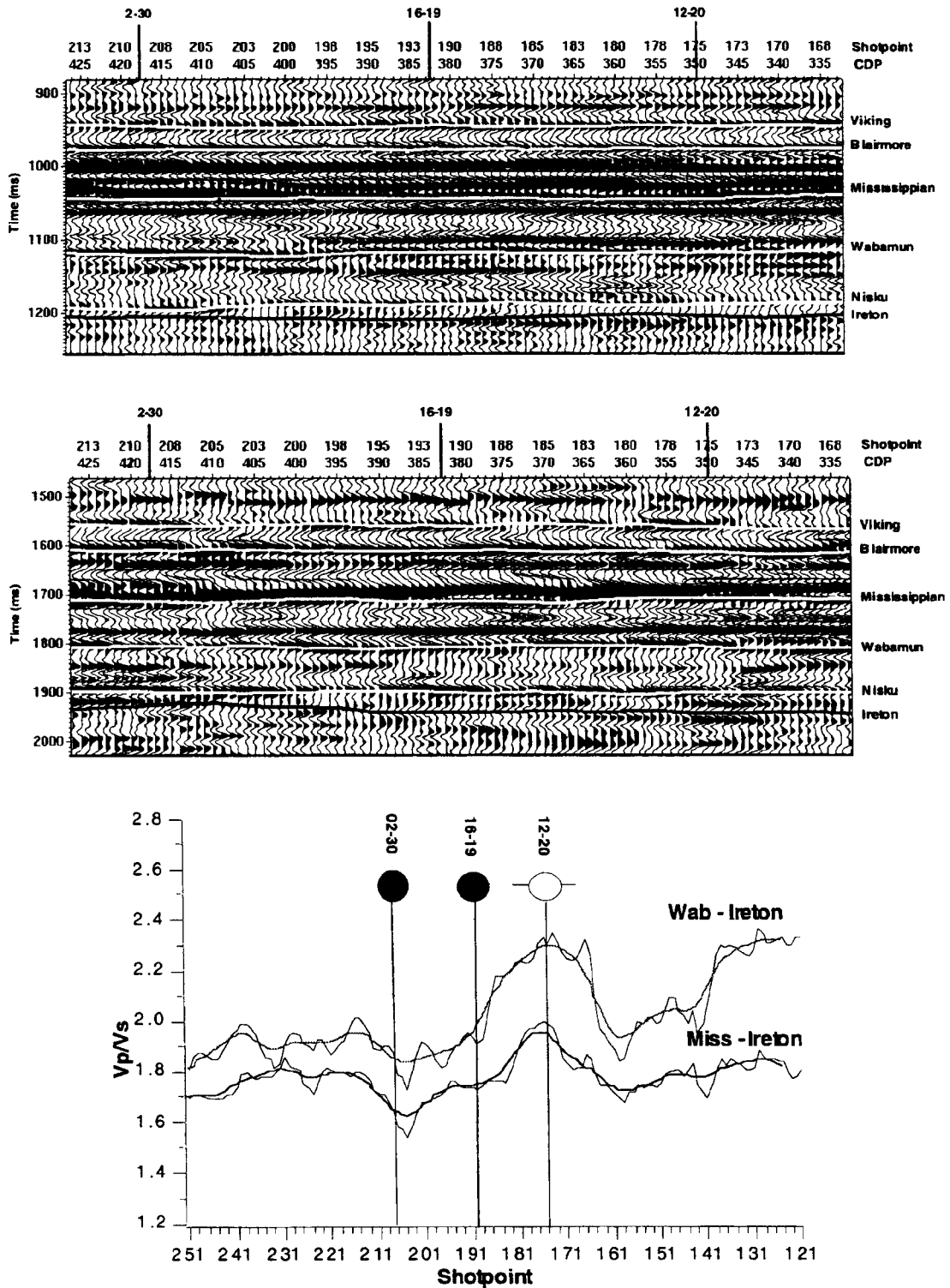


Fig. 20: P-P section (top) and P-S section (middle) from the Lousana field, Alberta. The  $V_p/V_s$  value (bottom) is extracted from the interpreted P-P and P-S sections. The lower values in the Paleozoic, from shot point 172 to 212, are coincident with an underlying oil-bearing reef (Miller et al., 1998).

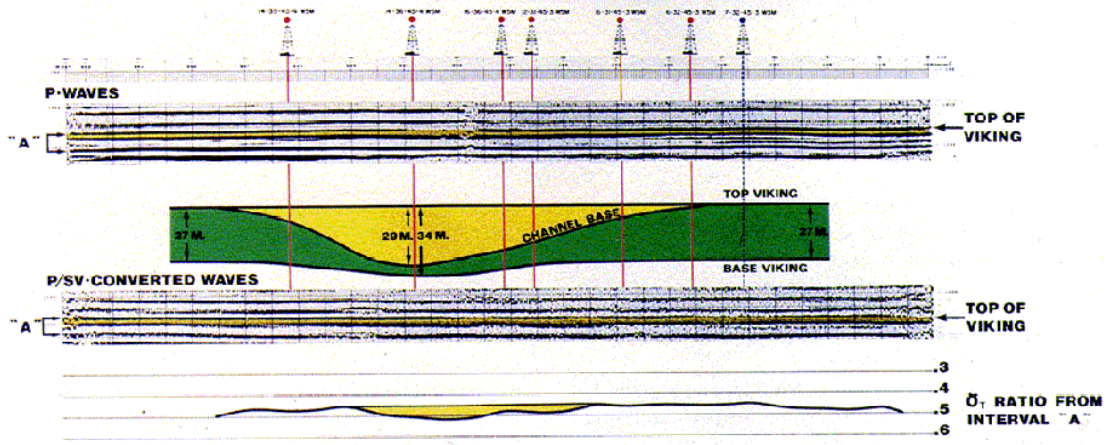


Fig. 21:  $V_P/V_S$  ( $\gamma_T$ ) anomaly over a Viking sand channel from P-P and P-S isochron ratios (Garotta et al., 1985).

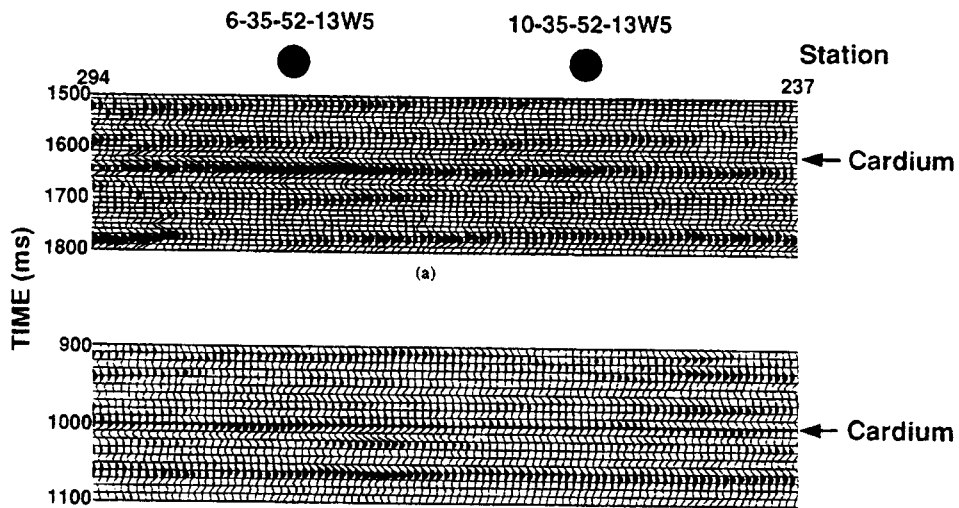


Fig. 22: Detail of the P-S (top) and P-P (bottom) sections from Carrot creek, Alberta. Note the amplitude anomaly on the P-S section at the Cardium conglomerate level (from Nazar and Lawton, 1993).

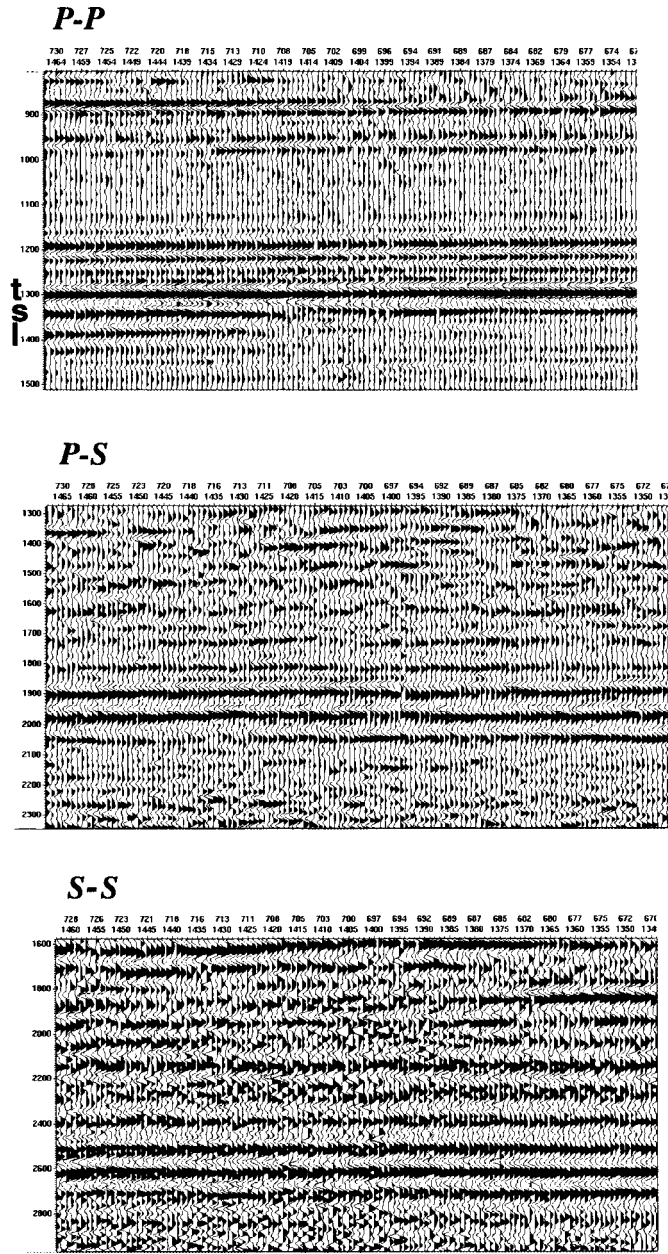


Fig. 23: P-P, P-S, and S-S data from a 9-C survey at Olds, Alberta. The P-wave data are of very good quality; the P-S section is somewhat less noisy than the S-S section (from Yang and Stewart, 1996).

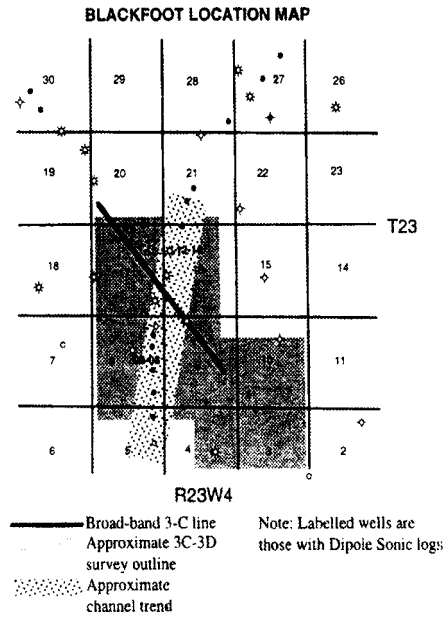


Fig. 24: Location map for the Blackfoot seismic experiments.

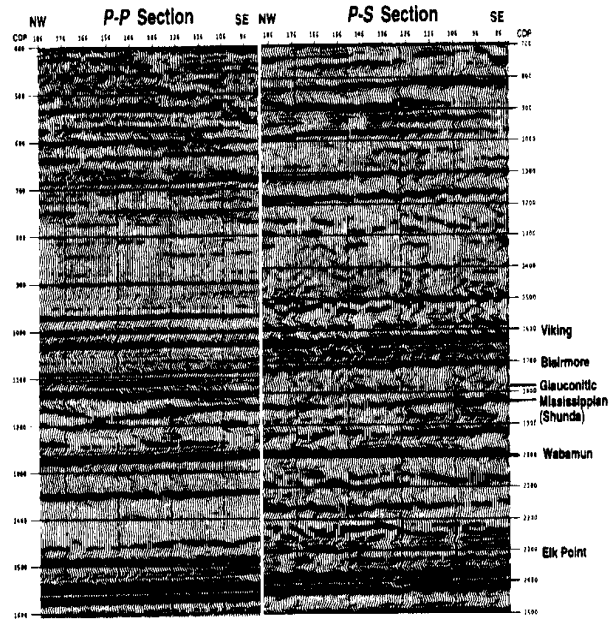


Fig. 25: Correlation of the broadband 2-D lines (P-P and P-S) over the Blackfoot field.

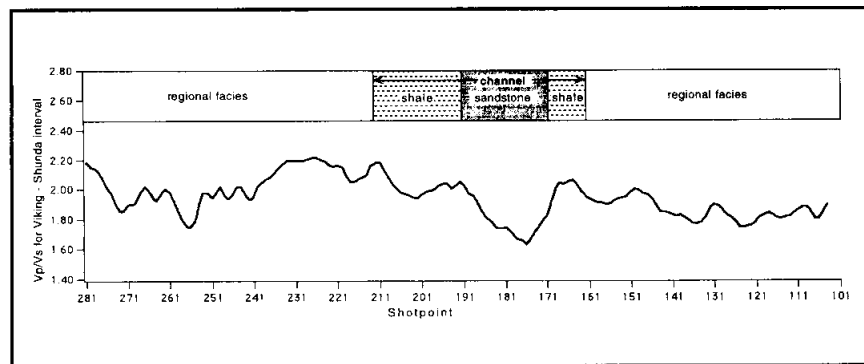


Fig. 26:  $V_p/V_s$  plot derived from P-P and P-S isochron ratios from the top of the Glauconite channel to the Wabamun level in the Blackfoot field. Low  $V_p/V_s$  values indicative of sand are shown in the light parts of the grey scale.

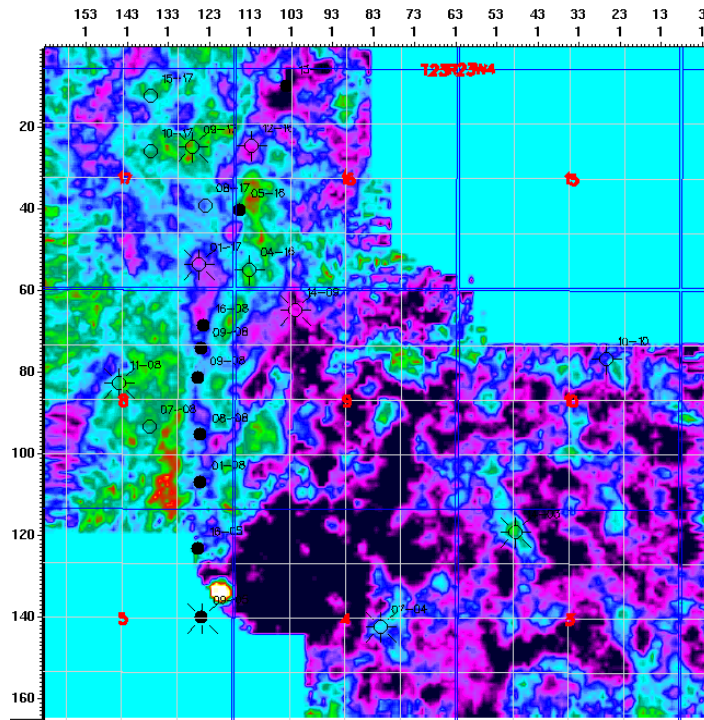


Fig. 27: P-P time slice on the interpreted top of the sand channel from the Blackfoot 3C-3D survey.

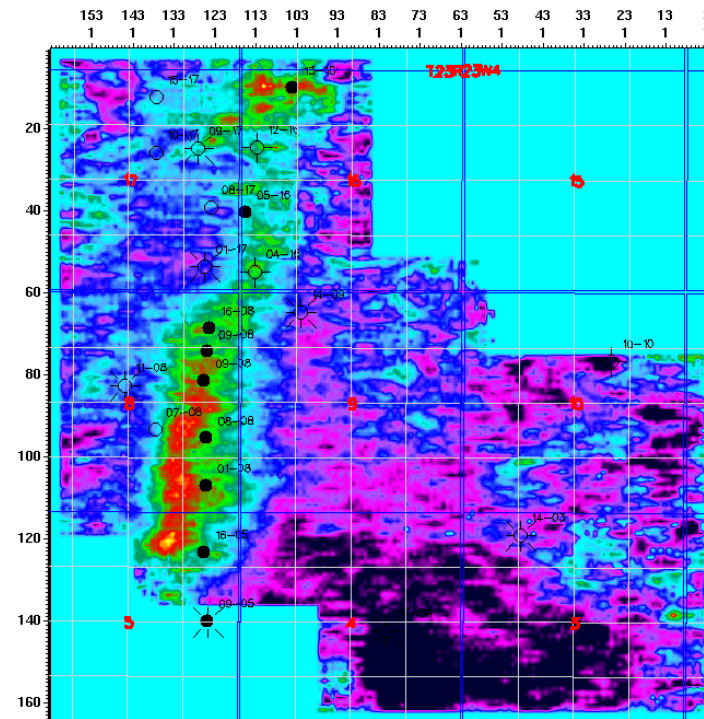


Fig. 28: P-S time slice at the interpreted sand channel level from the Blackfoot 3C-3D survey.

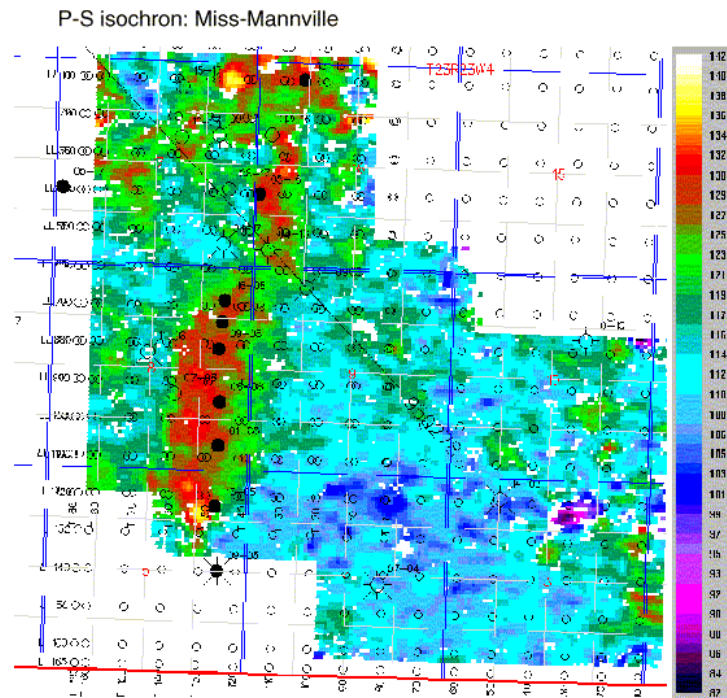


Fig. 29: P-S isochron between the Mannville to Mississippian horizons.

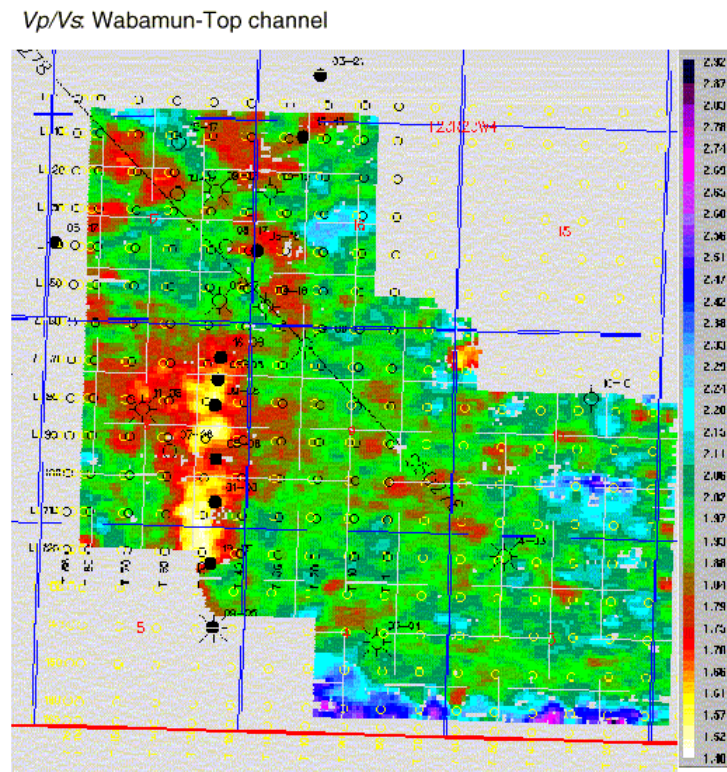


Fig. 30:  $V_p/V_s$  map for the reservoir region using a P-P and P-S isochron from the top of the channel to the Wabamun reflector (Top channel-Wabamun).

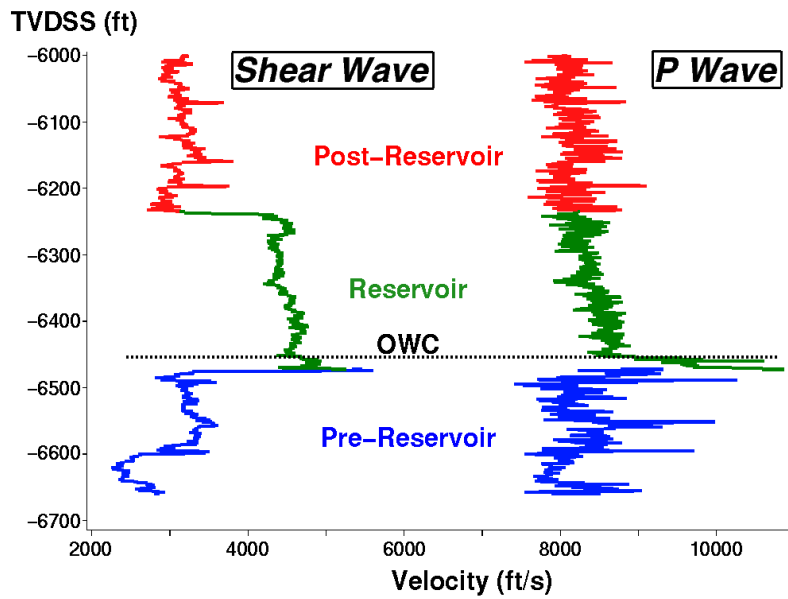
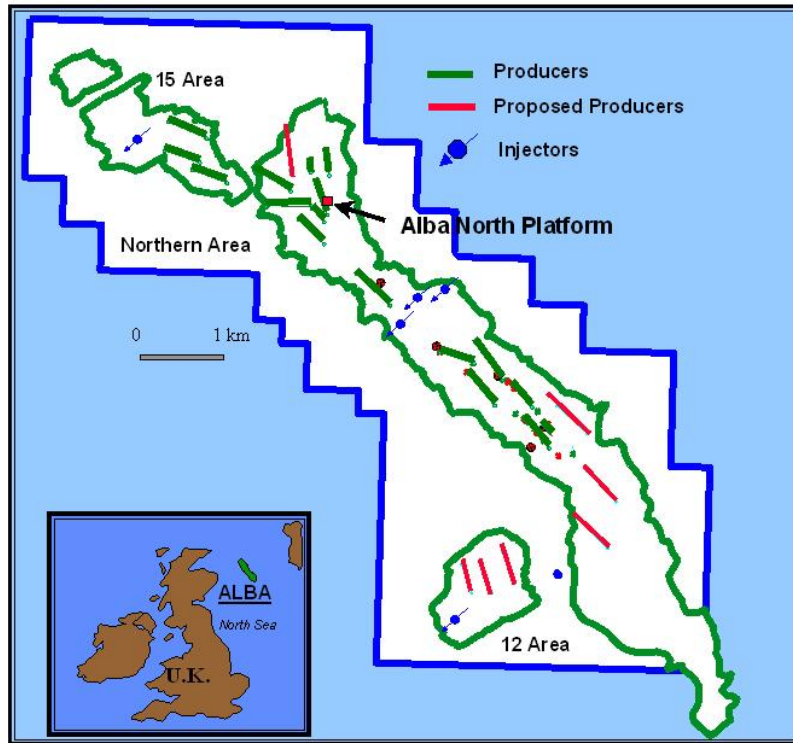
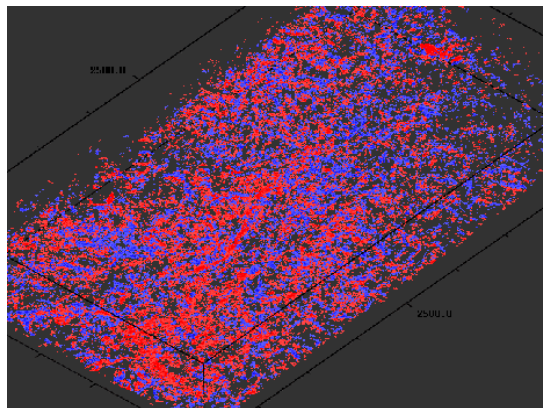
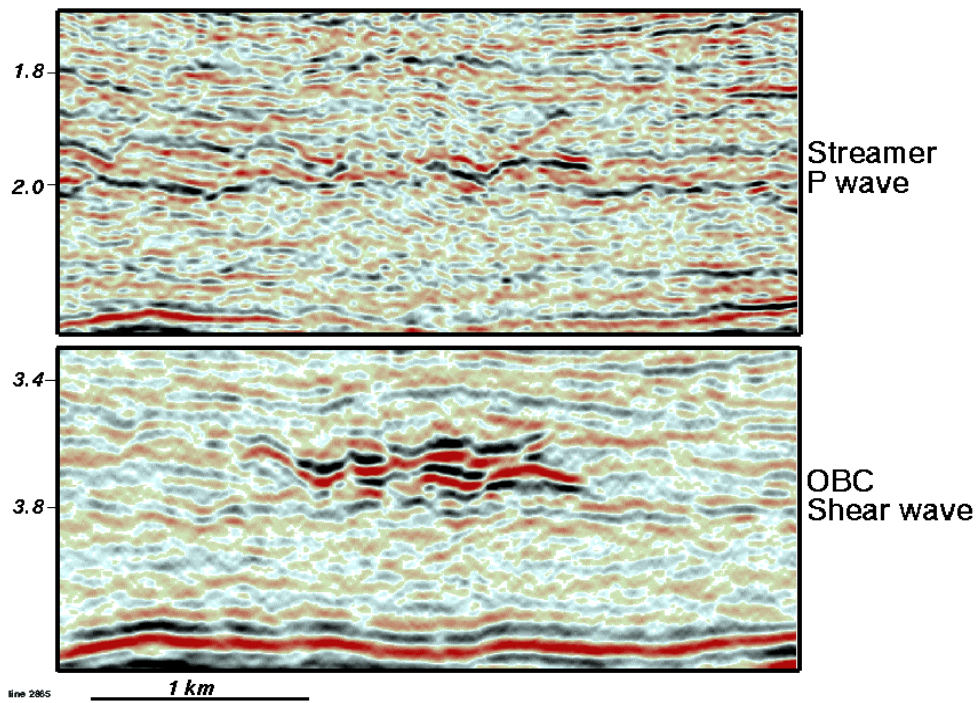


Fig. 31: Location and outline of the Alba field in the Central UK North Sea. On the right is a dipole sonic log through the Alba reservoir sand showing a large contrast in shear wave velocity and a small contrast in P-wave velocity with the surrounding shales (after MacLeod et al., 1999b).



Only high amplitudes displayed

**Streamer P wave**

**OBC Shear wave**

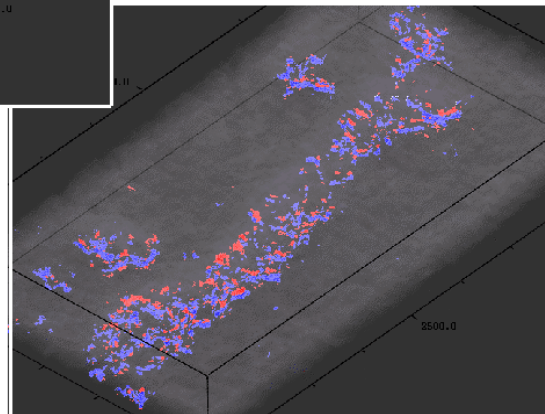


Fig. 32: Converted-wave image from the “15 Area” (see Figure 31) showing dramatically improved imaging relative to the streamer P-wave data. On the right is a 3D view of the streamer and converted-wave OBC data over Alba field. In each display, a sub-volume of the original data is displayed with only the high amplitudes visible. The outline of the Alba field is clearly seen only in the converted-wave data (after MacLeod et al., 1999b).

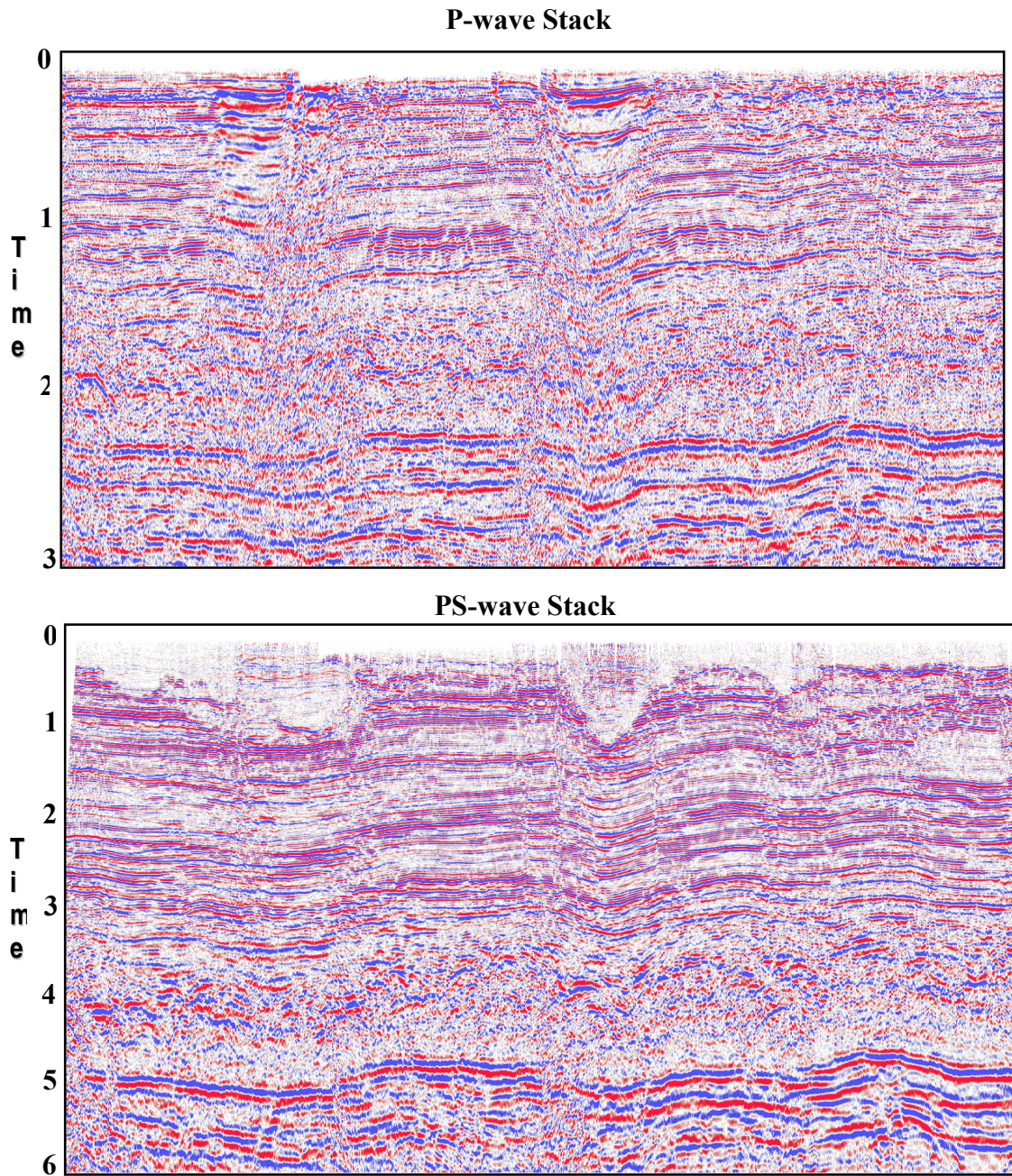


Fig. 33: Comparison between P-wave and P-S 2-D section over North Sea shallow-gas channels. P waves exhibit reverberations and high-frequency attenuation, but P-S section delineates the channel base, interfaces below the channel, and even sediment boundaries within the channel.

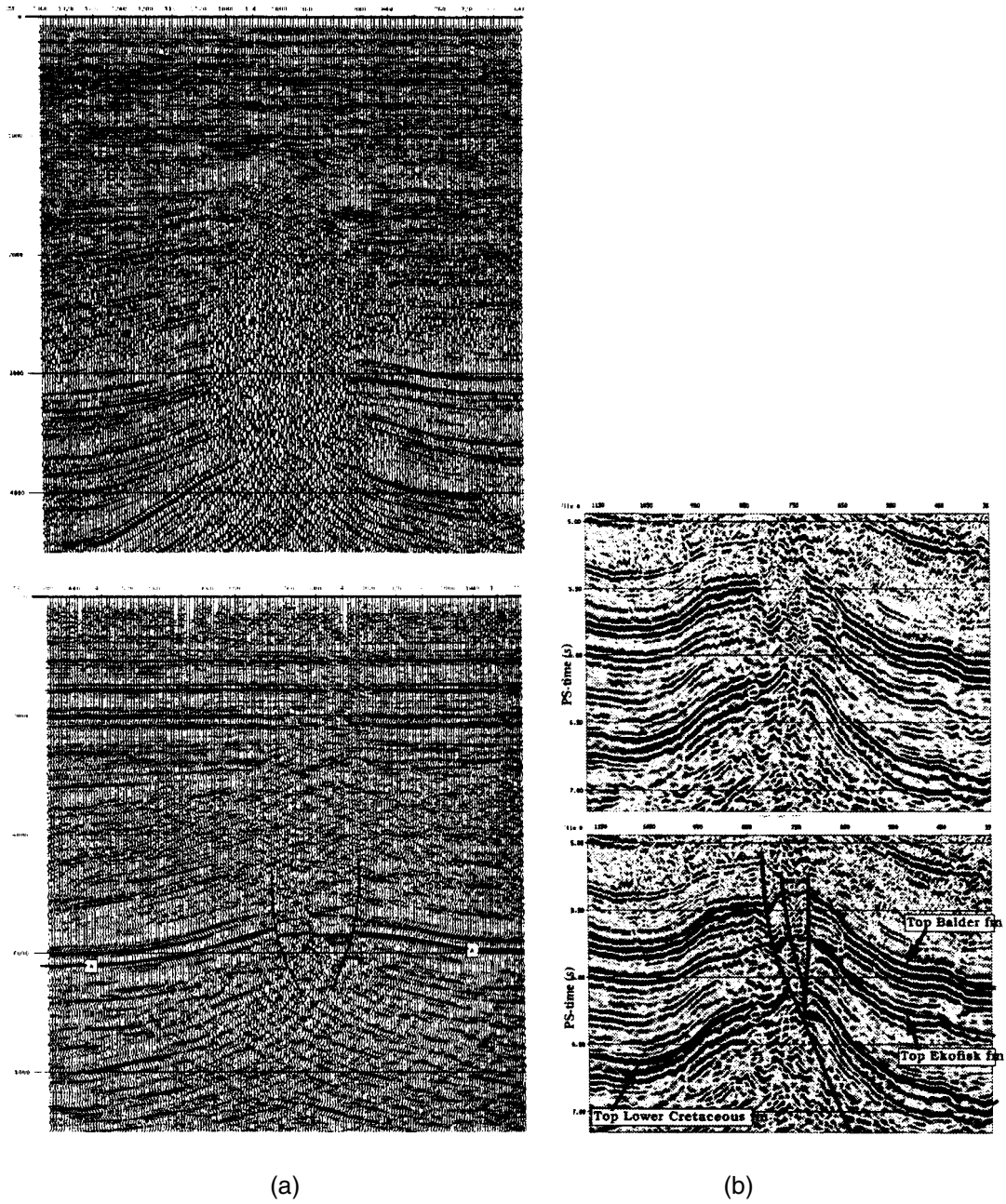


Fig. 34 (a): P-wave data from the North Sea using a streamer (top) and a SUMIC S-wave section (bottom) from Berg et al. (1994). (b): SUMIC P-S wave sections with and without interpretation (Granli et al., 1995).

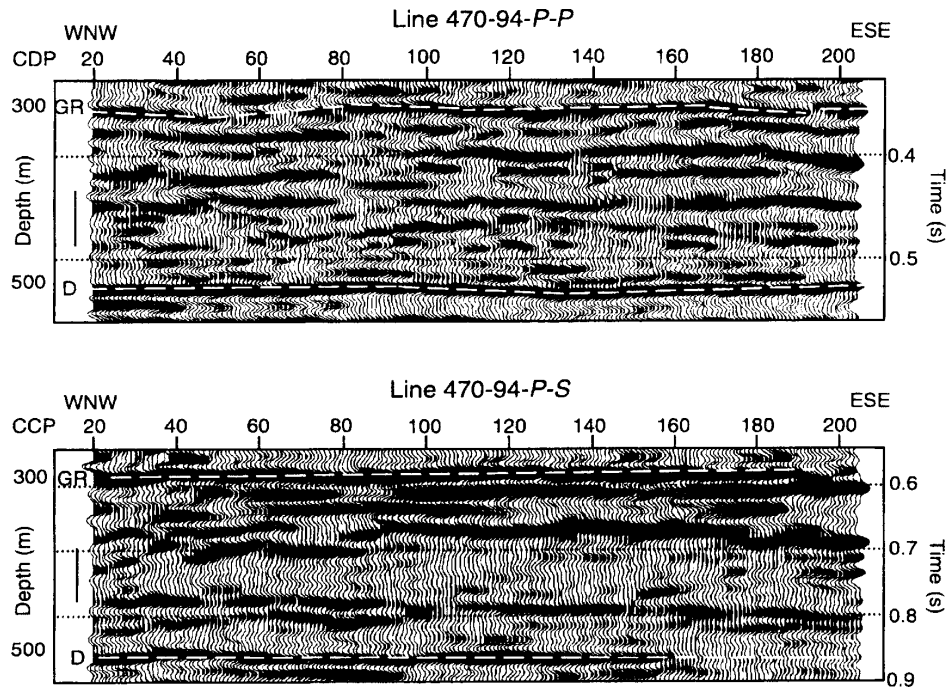


Fig. 35: P-P and P-S seismic lines from Cold Lake, Alberta. Time picks on the Grand Rapids formation (GR) and top of the Devonian are indicated (from Isaac, 1996).

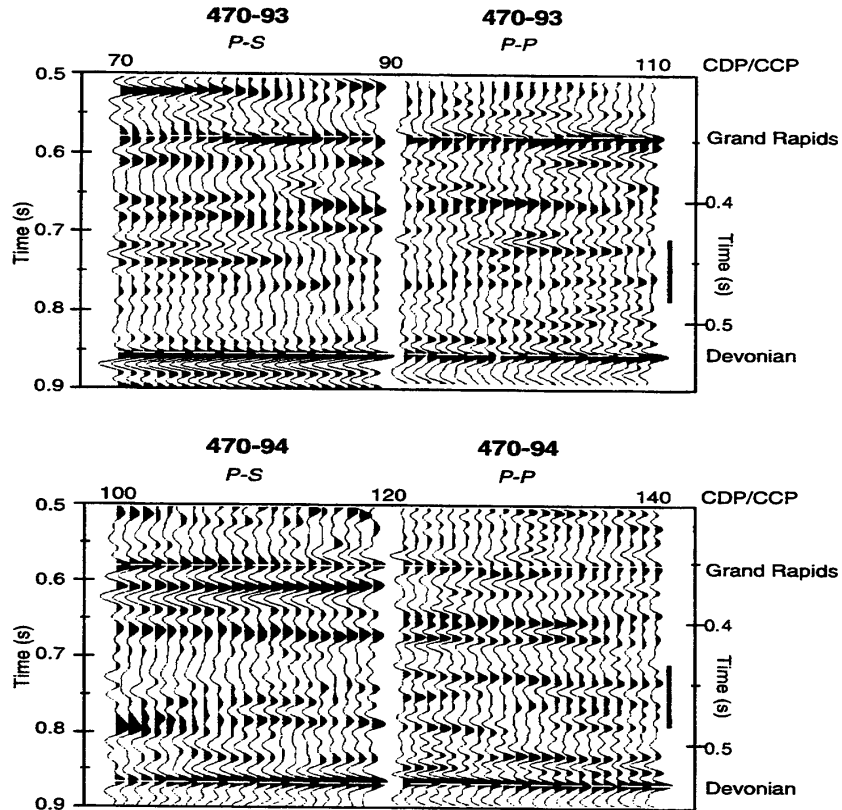


Fig. 36: Comparison of the 1993 and 1994 seismic lines. Note the similar data quality and resolution among all lines (from Isaac, 1996).

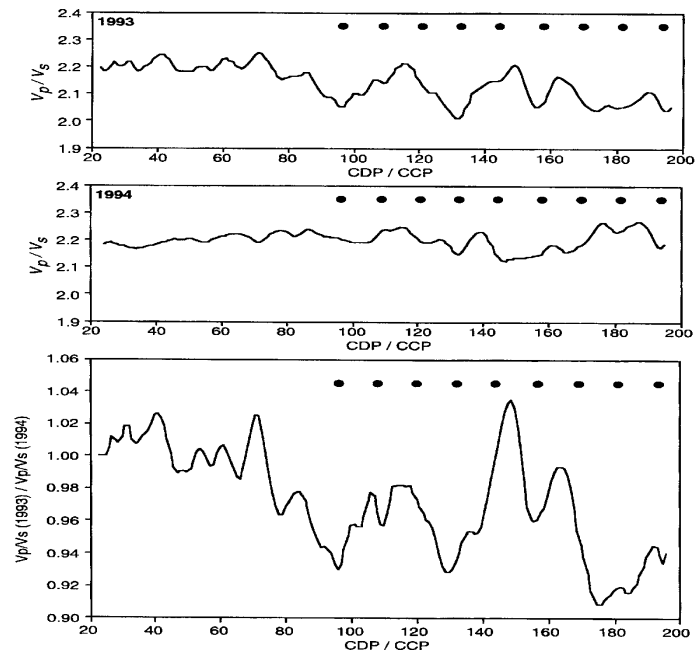


Fig. 37:  $V_p/V_s$  plots for 1993 lines, 1994 lines, and the ratio of those two. Note that the  $V_p/V_s$  value is generally lower in the unsteamed regions away from the wells (from Isaac, 1996).

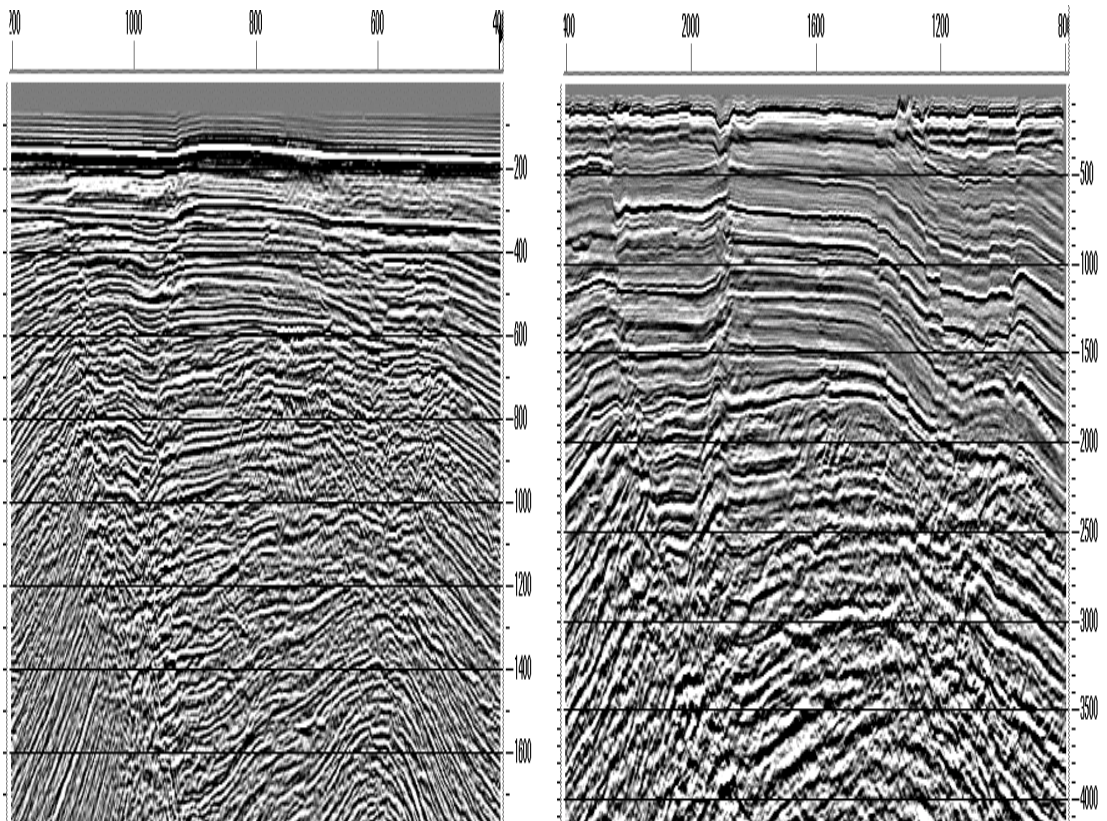


Fig. 38: (a) Post-stack migrated stack of geophones component from the Mahogany field. (b) Post-stack time migration of depth-variant CCP stack of X-component from the Mahogany field.

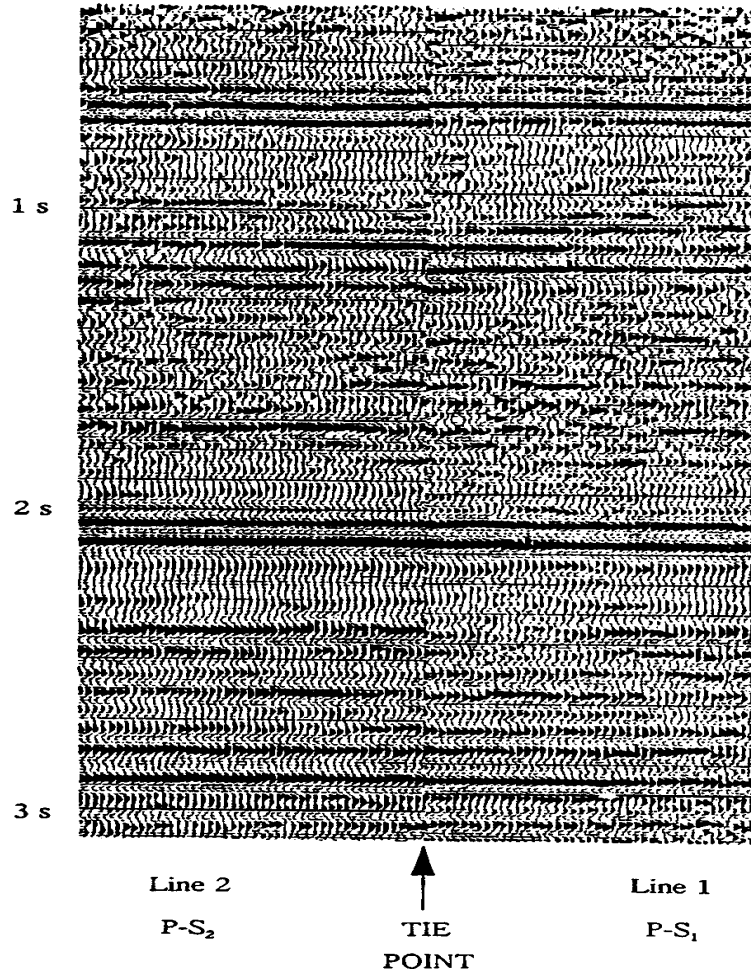


Fig. 39: P-S<sub>1</sub> (fast direction) and P-S<sub>2</sub> (slow direction) sections from the Willesden Green area of Alberta. No obvious anisotropy is apparent.

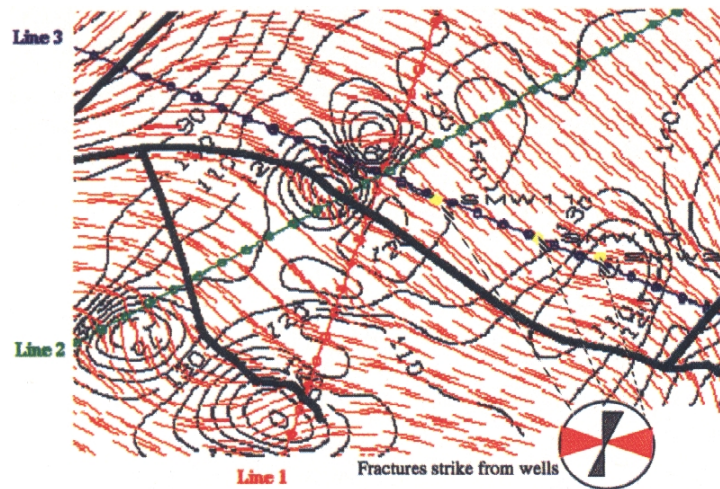


Fig. 40: Contoured fracture direction as determined from the fast direction of P-S data, from 3 crossed seismic lines (Ata and Michelena, 1995).

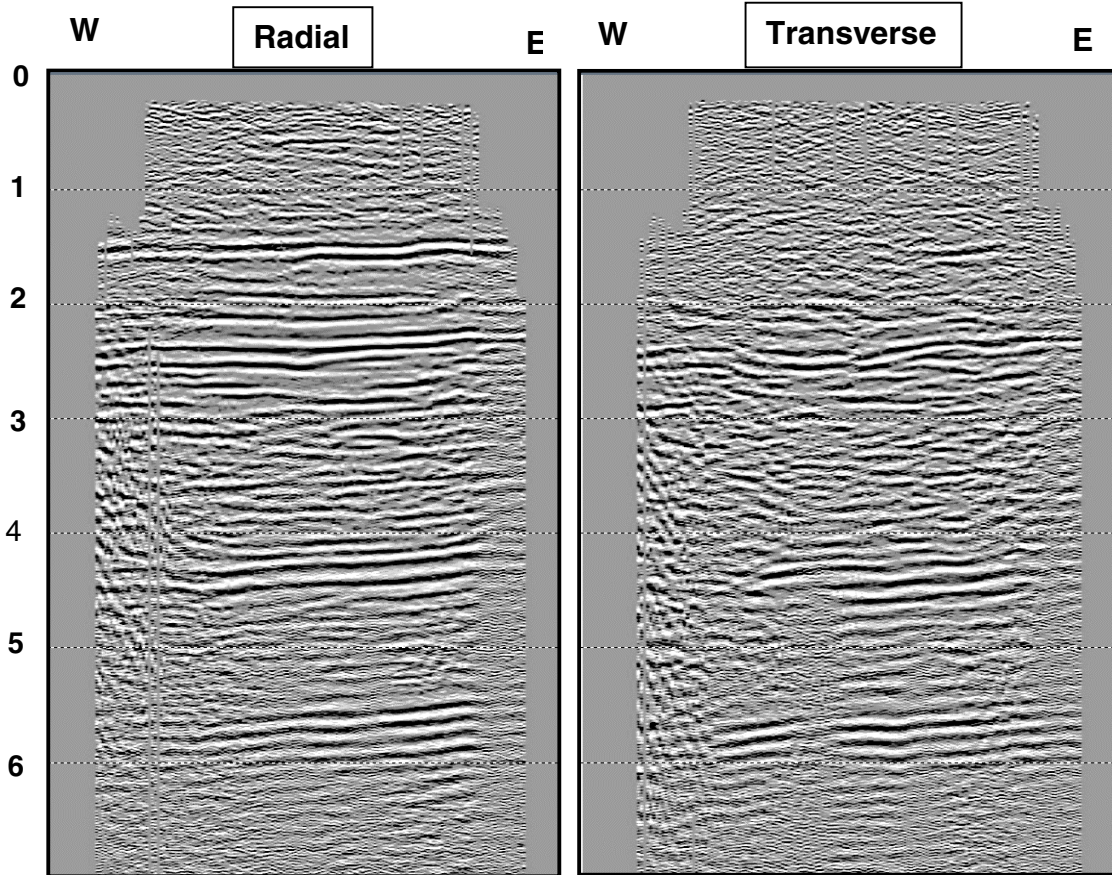


Fig. 41: Radial and transverse receiver components for east-west propagation from a 3-D survey at the Madden field in Wyoming. Using equivalent sections for north-south propagation, 4-component Alford rotations and layer stripping are performed to give the results in Figure 42.

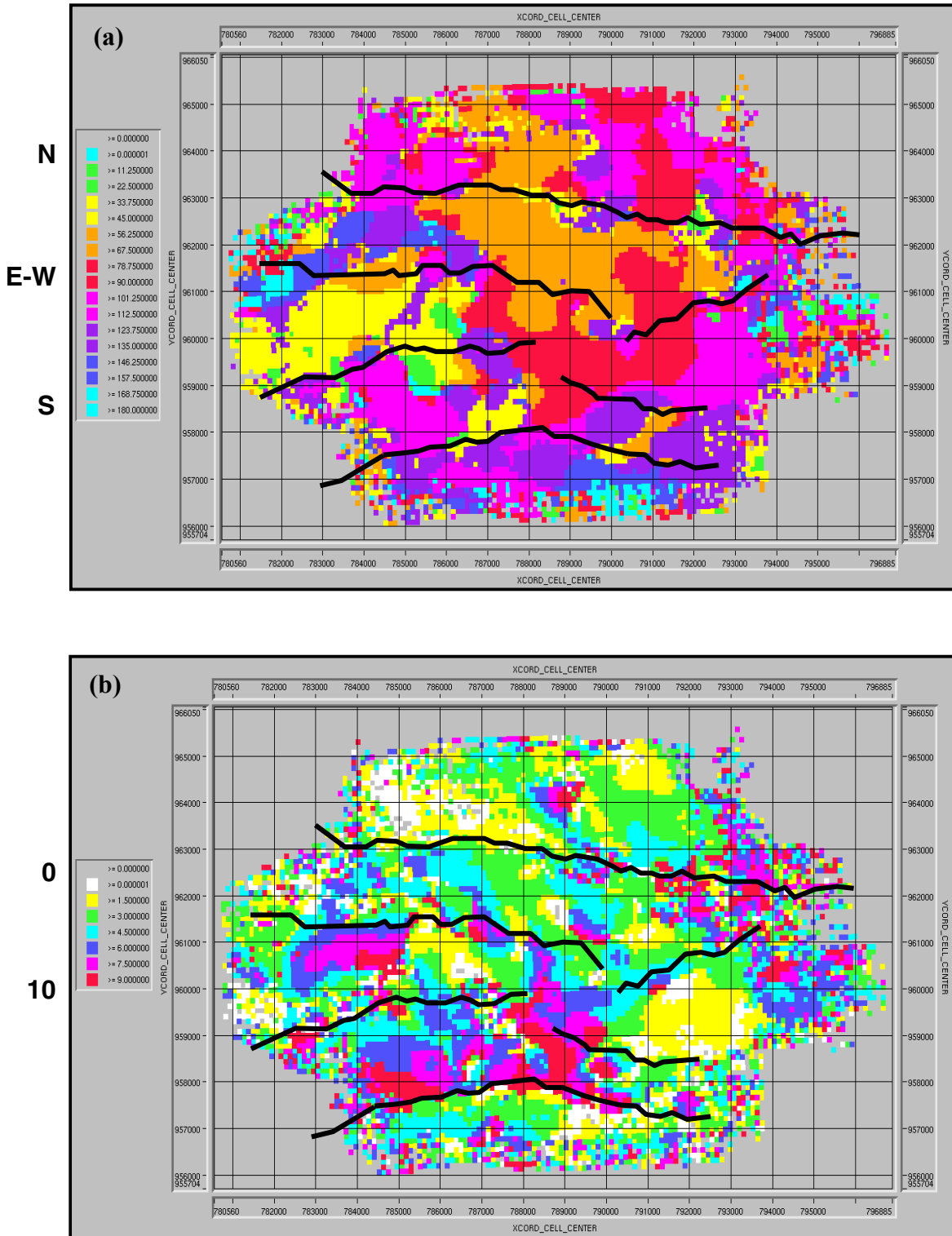


Fig. 42: Seismic anisotropy calculated by Alford rotation and layer stripping from the data in Figure 41, after removing the birefringence effects of the overburden. Fast S-wave (P-S1) polarization direction (a) and percent azimuthal anisotropy (b) for the target layer between 2.2 and 3.3 s. Regions of high percent anisotropy (9% or more) correlate well with the known east-west trending faults superimposed on the maps.

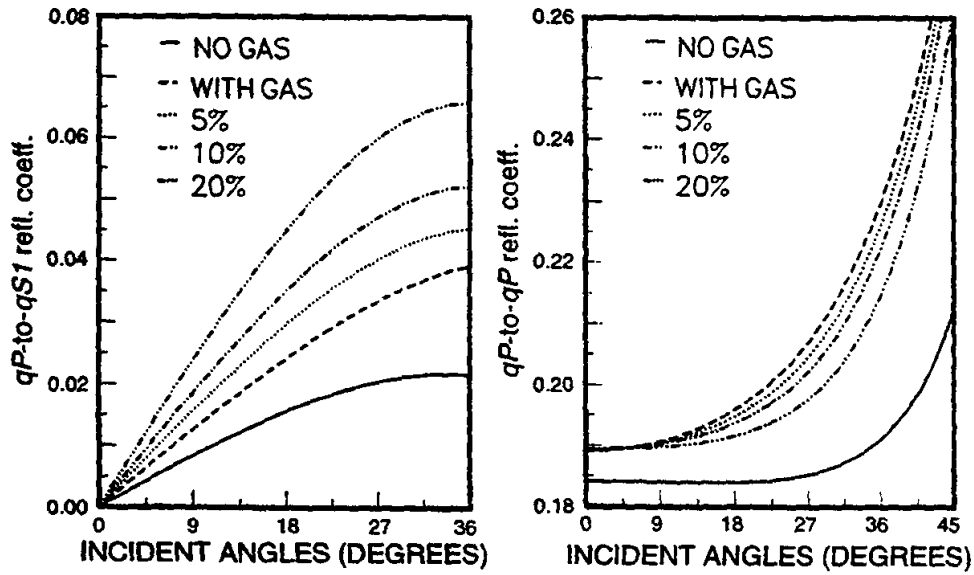


Fig. 43: Theoretical modelling for gas-saturated fractured material indicating that anisotropy may have a large effect.

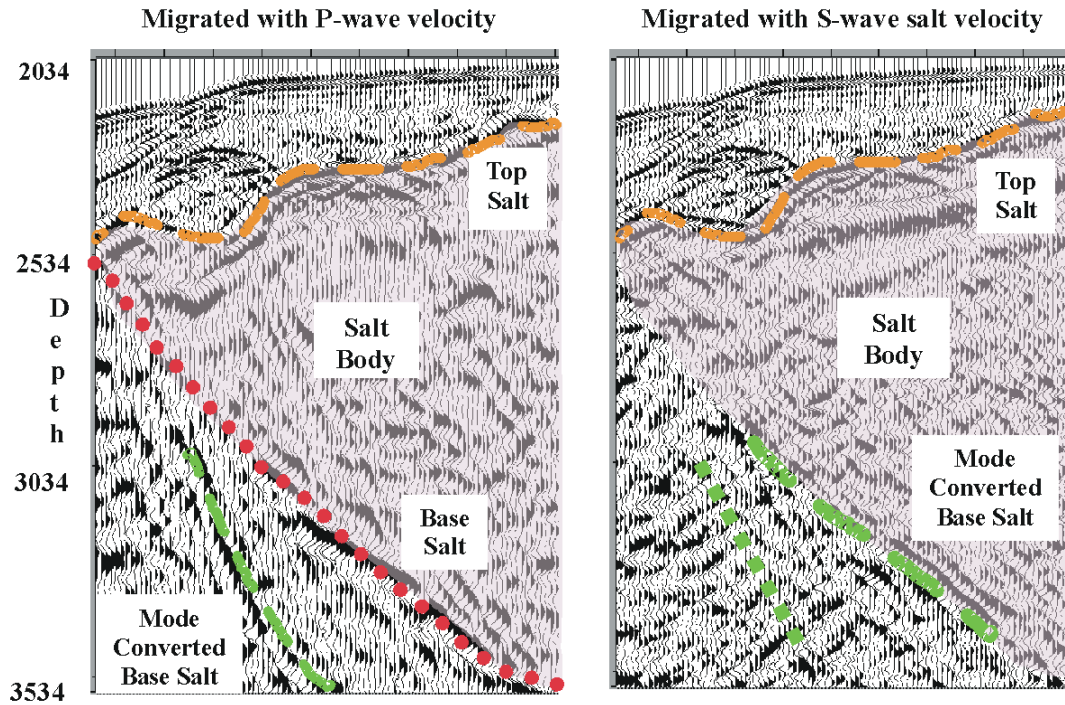


Fig. 44: Comparison of prestack depth-migrated streamer data using P-wave and S-wave salt-velocity models. Migration with an S-wave velocity model images PSSP waves that have converted at top salt. Position of the S-wave base-salt event is in agreement with the P-wave image.